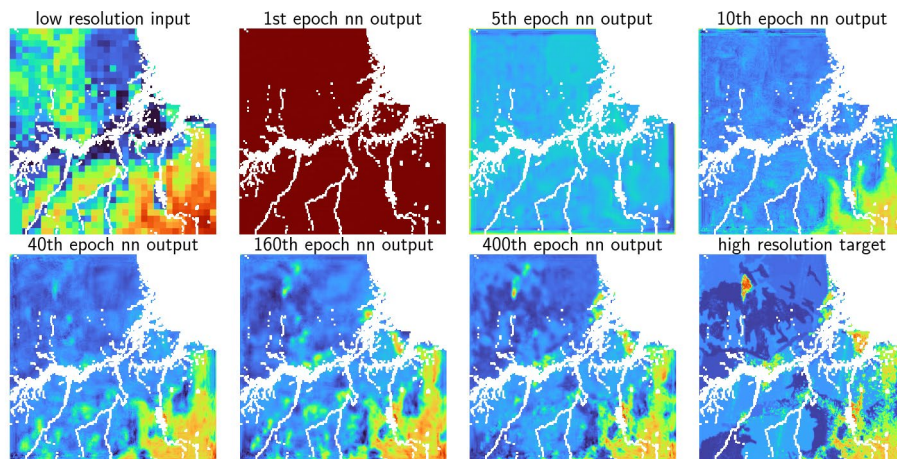


TOOLS OF THE TRADE

A clearer view of Earth's water cycle via neural networks and satellite data

To manage and protect water resources, it is necessary to understand the water cycle. Passive microwave radiometers onboard satellites are used to monitor water resources, like soil moisture. However, microwave sensors, such as radiometers, are too coarse to see small-scale meteorological features, which can affect large-scale phenomena occurring within the water cycle. Other spaceborne instruments produce finer-resolution images, but these instruments are much more sensitive to cloud contamination, limiting their useful coverage.



Data from Kim, S. et al. 2016. SMAP L3 Radar Global Daily 3 km EASE-Grid Soil Moisture, Version 3. April 13–July 7th, 2015 NSIDC Distributed Active Archive Center <https://doi.org/10.5067/IGQNPB6183ZX> (2016) and O'Neill, P.E. et al. 2021. SMAP L3 Radiometer Global Daily 36 km EASE-Grid Soil Moisture, Version 8. April 13–July 7th, 2015. NSIDC Distributed Active Archive Center <https://doi.org/10.5067/OMHVSRCFX38O> (2021) accessed March 26, 2022.

Neural networks provide an opportunity to build on the global coverage of radiometers by improving their spatial resolution. These networks are a classic methodology in machine learning, taking input and target data pairs and drawing an algorithm connecting the two. To enhance radiometer data from freely available historical environmental datasets acquired from satellite missions such as Aqua, SMAP, and the upcoming SWOT mission, low-resolution images are fed into a very deep neural network. The neural net starts out untrained, taking the input data and turning it into noise. This noise is

compared to the desired high-resolution target, and the machine learning framework updates the prediction algorithm based on the comparison. This loop of prediction and refinement is performed many times until the now trained network accurately produces high-resolution images from the original low-resolution satellite radiometer data. These refined images can then be used to better track changes in the water cycle.

Although the mechanics of neural networks have been around for decades, their application in water science has become more popular with the advent of open-source software and inexpensive high-powered computing. Enhanced resolution microwave radiometer products are increasingly vital to the geoscience community. For example, higher-resolution soil moisture data (like that in the graphic showing a neural network training process at the mouth of the Amazon River) will improve numerical weather prediction, drought analysis, crop yield planning, and flood forecasting. A detailed, clearer view of the water cycle resulting from applying neural networks will support more sustainable management of water resources.

Albert Larson 

Department of Civil and Environmental Engineering,
University of Rhode Island, Kingston, RI, USA.

e-mail: albert@uri.edu

Competing interests

The author declares no competing interests.



Article

Discerning Watershed Response to Hydroclimatic Extremes with a Deep Convolutional Residual Regressive Neural Network

Albert Larson ¹, Abdeltawab Hendawi ², Thomas Boving ^{1,3}, Soni M. Pradhanang ³ and Ali S. Akanda ^{1,*}

¹ Department of Civil and Environmental Engineering, University of Rhode Island, Kingston, RI 02881, USA; alarson0015@gmail.com

² Department of Computer Science and Statistics, University of Rhode Island, Kingston, RI 02881, USA

³ Department of Geosciences, University of Rhode Island, Kingston, RI 02881, USA

* Correspondence: akanda@uri.edu

Abstract: The impact of climate change continues to manifest itself daily in the form of extreme events and conditions such as droughts, floods, heatwaves, and storms. Better forecasting tools are mandatory to calibrate our response to these hazards and help adapt to the planet's dynamic environment. Here, we present a deep convolutional residual regressive neural network (dcrrnn) platform called Flux to Flow (F2F) for discerning the response of watersheds to water-cycle fluxes and their extremes. We examine four United States drainage basins of varying acreage from smaller to very large (Bear, Colorado, Connecticut, and Mississippi). F2F combines model and ground observations of water-cycle fluxes in the form of surface runoff, subsurface baseflow, and gauged streamflow. We use these time series datasets to simulate, visualize, and analyze the watershed basin response to the varying climates and magnitudes of hydroclimatic fluxes in each river basin. Experiments modulating the time lag between remotely sensed and ground-truth measurements are performed to assess the metrological limits of forecasting with this platform. The resultant mean Nash–Sutcliffe and Kling–Gupta efficiency values are both greater than 90%. Our results show that a hydrological machine learning platform such as F2F can become a powerful resource to simulate and forecast hydroclimatic extremes and the resulting watershed responses and natural hazards in a changing global climate.

Keywords: water; climate; sustainability; supervised representation learning; societal considerations



Citation: Larson, A.; Hendawi, A.; Boving, T.; Pradhanang, S.M.; Akanda, A.S. Discerning Watershed Response to Hydroclimatic Extremes with a Deep Convolutional Residual Regressive Neural Network. *Hydrology* **2023**, *10*, 116. <https://doi.org/10.3390/hydrology10060116>

Academic Editors: Ali A. Assani and Arona Diedhiou

Received: 31 March 2023

Revised: 5 May 2023

Accepted: 18 May 2023

Published: 23 May 2023



Copyright: © 2023 by the authors. Licensee MDPI, Basel, Switzerland. This article is an open access article distributed under the terms and conditions of the Creative Commons Attribution (CC BY) license (<https://creativecommons.org/licenses/by/> 4.0/).

1. Introduction

Water is connected to and connects all living things on Earth. It is wielded to power electronic devices, enables plants, food, and animals to grow, serves as the living and recreational space for all creatures, and is nourishment to the human body. It has been both the subject of, platform for, and weapon of choice in numerous conflicts. Global hydraulic infrastructure is highly variable. Dirty water can be a source of disease and death. It is branded, modified, and sold at differing levels of purity and concentration. The cost of equipment to control the flow of water is high, maintenance is frequent, and changes in demand and supply for water as a resource are constant sources of concern.

Human activities have changed and continue to change Earth's environment. The changes are visible in both short- (meteorological) and long- (climatological) time scale observations [1]. As the temperature of our home planet increases, the amount of snow and sea ice loses volume over time [2,3], sea levels rise and swallow up once inhabited land [4,5], storms intensify [6], droughts last longer [7], floods become more severe [8,9], animal populations go extinct [10], and the availability of freshwater becomes more unreliable [11]. Concurrently, manmade Earth observation and control systems continue to improve [12,13].

Watershed modeling is an important field of research that involves predicting the movement of water through the Earth's system. Earth's system consists of the land, atmosphere, and ocean. Many models have been developed to simulate and predict hydrologic processes, including rainfall, runoff, and evapotranspiration [14]. One popular model is the Soil and Water Assessment Tool (SWAT), which has been used extensively to model hydrology and water quality in watersheds [15,16]. Another model, the Variable Infiltration Capacity (VIC) model, has been employed to study changes in streamflow and soil moisture [17]. General circulation models (GCMs) are an additional important tool in hydrology modeling. GCMs simulate the Earth's climate system, including atmospheric circulation, ocean circulation, and the cryosphere, and provide predictions of future climate conditions [18]. These models have been used to study the impacts of climate change on water resources and hydrologic processes, such as changes in precipitation patterns and snowmelt runoff [19]. In addition, GCMs can be coupled with regional ocean modeling systems (ROMS) to study ocean circulation and its impact on coastal ecosystems [20]. The Massachusetts Institute of Technology General Circulation Model (MITgcm) is another popular model used to simulate ocean circulation and study the impacts of climate change on marine ecosystems [21].

Here, we approach the topic of watershed modeling with a deep neural network. We observe the connections between the model output of four United States drainage basins to actual in-river. All basins are larger than a million acres and thus provide ample data to observe how changes in the runoff and subsurface flow impact the quantity of water discharging from the major river within the basin. We also see the tools being translated to other domains and languages. This work is significant for two major technical reasons. The first reason is because of its application of modern technologies (neural networks, graphical processing units, jupyter notebooks) to a classic hydrology problem. These tools are both shown to be capable of high performance, whilst fluid to read and easy to use. The second reason is because of the white-box, open-source constraint we imposed upon the work of the experiments. Given our results, we envision future work applying the same tools to study and consider all of Earth's watersheds at fine fidelity.

2. Materials and Methods

The F2F code base provides an in-depth view of the materials and methods applied within. As such, it is a key of part of the work and has been made openly accessible at <https://github.com/albertlarson/f2f> (accessed on 30 March 2023). The scripts follow the logical order of this paper. Specifically, these notebooks serve as the vessel to start with time-series preprocessing and neural network building and analysis. Furthermore, we have selected a cross-section of the pertinent information below.

2.1. Study Areas

Four United States drainage basins with areas of greater than one million acres each were selected as study areas and are shown in Figure 1. The Bear River and Connecticut River watersheds are significantly smaller than either the Mississippi River or the Colorado River basins. The satellite imagery used observes approximately 100 square kilometers of area (on the order of 25,000 acres) in each pixel.

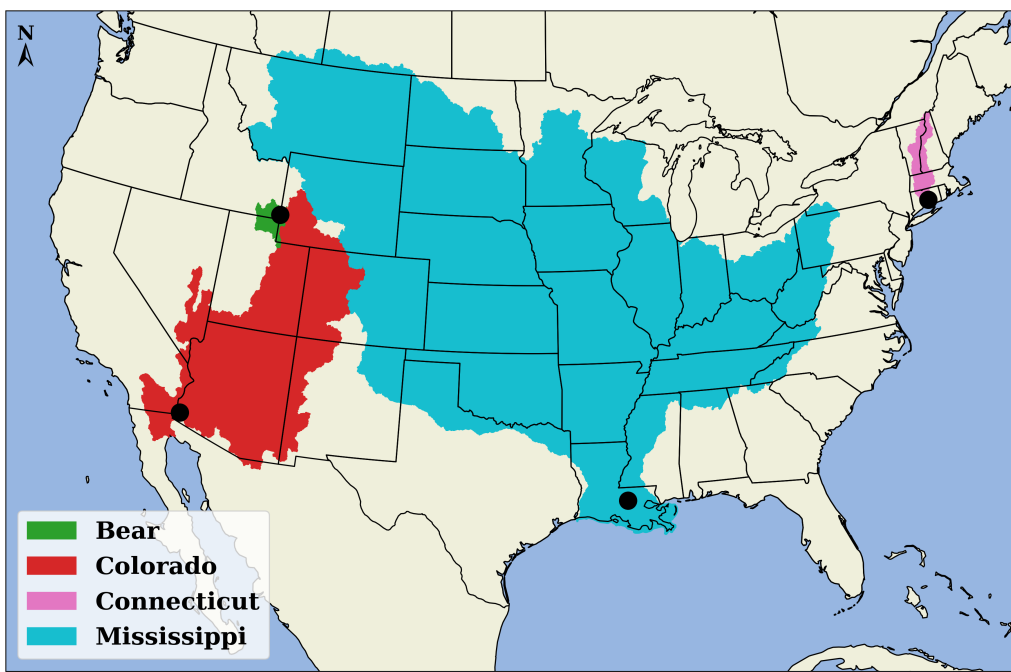


Figure 1. Drainage basins under investigation (not to scale).

2.2. Satellite-Derived Observations

For each basin there are two input images extracted from raw data obtained through the NASA Goddard Earth Sciences Data and Information Services Center. The raw data are National Land Data Assimilation System (NLDAS) model output. The NLDAS is a project run by several United-States-based institutions and universities. The NLDAS takes continental-scale meteorological data parameters (e.g., air temperature, wind speed, surface pressure, precipitation, incoming radiation, specific humidity) as input and deterministically creates water- and energy-flux layers as outputs. The NLDAS project in its second phase applies several different water- and energy-balance algorithms to create flux outputs from one common set of meteorological inputs. Here, the Noah water- and energy-budget algorithm is used. The channels of interest are components of the water flux, specifically the surface and subsurface runoff, as they collectively represent the lateral movement of liquid water along and under the surface towards the terminal drainage point at a given point in time [22,23].

2.3. Ground-Truth Measurements

Concurrent with the two NLDAS channels is a single gauged-in-the-river streamflow measurement. Daily streamflow measurements from sites near the terminus of each basin are obtained from the United States Geological Survey's National Water Information System. The sites were selected based on the availability, proximity to the terminal point of the basin, and relative continuity of the data. Gaps in the data collection are solved with linear interpolation.

Ground-truth streamflow data are critical for hydrologic modeling, as they provide a means of validating and calibrating model results. The USGS National Water Information System (NWIS) is a primary source of ground-truth streamflow data in the United States [24]. The NWIS is a network of over 1.5 million sites that collect measurements of water, some of which are then used to calculate streamflow [25]. These gauges are operated by the USGS in collaboration with other federal, state, and local agencies, as well as private organizations. The data collected by the NWIS are used for a wide range of applications, including flood forecasting, water management, and environmental assessments [26].

The NWIS stream gauges provide a valuable resource for monitoring and managing the nation's water resources. The network covers a broad range of water bodies, including

rivers, streams, lakes, and reservoirs, and the data collected help to support a variety of water-related activities. For example, the streamflow data collected by the NWIS are used to support flood-forecasting efforts, which are essential for public safety and property protection. In addition, the data are used to assess water availability for agriculture, industry, and domestic use and to monitor the health of aquatic ecosystems.

The USGS has a long history of collecting and analyzing streamflow data, dating back to the late 19th century when the agency was established [27]. Since then, the network of stream gauges has expanded and become more sophisticated, incorporating new technologies such as acoustic Doppler current profilers and advanced telemetry systems [25]. The USGS has also played a key role in developing standardized methods for collecting, processing, and analyzing streamflow data, which have been adopted by other countries around the world [28]. Today, the USGS continues to operate and maintain the largest network of stream gauges in the United States, providing a valuable resource for hydrologic research and water resource management [26]. With the growing importance of water resource management and the increasing threat of climate change, the role of the NWIS in monitoring and managing the nation's water resources is more critical than ever.

2.4. Data Collection and Preprocessing

For this study, we looked at the time range starting on 1 January 2015, until the most recent output available, 1 March 2022. The NLDAS model output is available as a monthly and hourly product. We combine the hourly data available for surface and subsurface streamflow into a daily product. The raw hourly NLDAS product with all variables is a directory sized 351 gigabytes composed of 62,805 hourly files. The summing and extraction of lateral flows shrunk the total file size by a factor of more than 150. Each raw data file consumes 5.8 megabytes of disk space, while each daily surface and subsurface flow extraction was 822.7 kilobytes. The filtered data consume only 2.1 gigabytes and can easily be held on a graphical processing unit when trained with the neural network. The file size decreases further when clipped to a particular basin. The images are z-scored relative to themselves, while the gauged streamflow data are z-scored relative to the entire time series of seven years. Whitening has been shown to improve the performance of training a neural network [29,30].

2.5. Treatment

For this experiment, we constructed a deep convolutional residual regressive neural network. Our network selection was inspired by the strong performance of a similar structure in the task of image classification [31] and the hypothesis that this work might be transferred to a new domain [32]. The guiding research question behind the use of this structure was "How does the use of a state-of-the-art stochastic model fare in the job of streamflow prediction typically reserved for deterministic methods such as the Saint-Venant equations [22] or the Muskingum model [33]?" The images of Earth's surface and subsurface water flow we obtain from NLDAS are passed through this network. Eventually, the transformed images reach a destination where the image shapes have been constrained in size to match that of the target of the input pair; here, the target is one pixel as the daily value for gauged streamflow is a single physical measurement. Shape transformation is a common occurrence in the application of neural networks, where one constrains an input shape to a target output shape. This is performed with different "layers", where some linear computations are performed based on the user-specified shape of the neural network. There are helpful resources for these fundamentals [34]. The problem is one of regression because the prediction of streamflow is continuous and can theoretically be any value greater than zero. We use convolutional neural networks because our input to the network is a sequence of two channel images [35]. We also use residual learning, which allows us to make the network very deep but control the opacity of the initial structure of the image. This makes training faster [31]. Rectified linear unit activation functions are applied in all but the last layer of nodes, and batch normalization is used in the residual

layers [36,37]. Batch normalization is like the z-score treatment in our preprocessing step. Finally, we selected a variant of stochastic gradient descent for optimization of the neural network nodes [38,39].

The gauged streamflow measurements of the four target rivers are significantly different in magnitude from one another; therefore, we process each with a z-score treatment to center their mean values around the number zero and standardize each increasing and decreasing integer around intervals of standard deviation. Figure 2 shows plots of the gauged streamflow measurements of each basin oriented in two ways. The four individual strip charts in the top right show the change in streamflow over time. The more prominent normal-distribution-shaped plots show how often actual measurements in the respective basin occur relative to the average discharge of each basin. This is a single-dimensional z-scoring system. We also perform a two-dimensional treatment on each of the input channels, surface, and subsurface streamflow. Whereas the 1D treatment uses the entire time series of gauged streamflow measurements for computation, the 2D z-scores are computed based on a single image at a time. The modifiable hyperparameter controls of the network are the basin under observation, the lag in time between the input and output datasets, the number of training epochs (forward and backward passes of the neural network), and the ratio of training data to testing data. There is also an override for stopping the model training early when the training data have a Nash–Sutcliffe efficiency (NSE) value of a variable efficiency percentage.

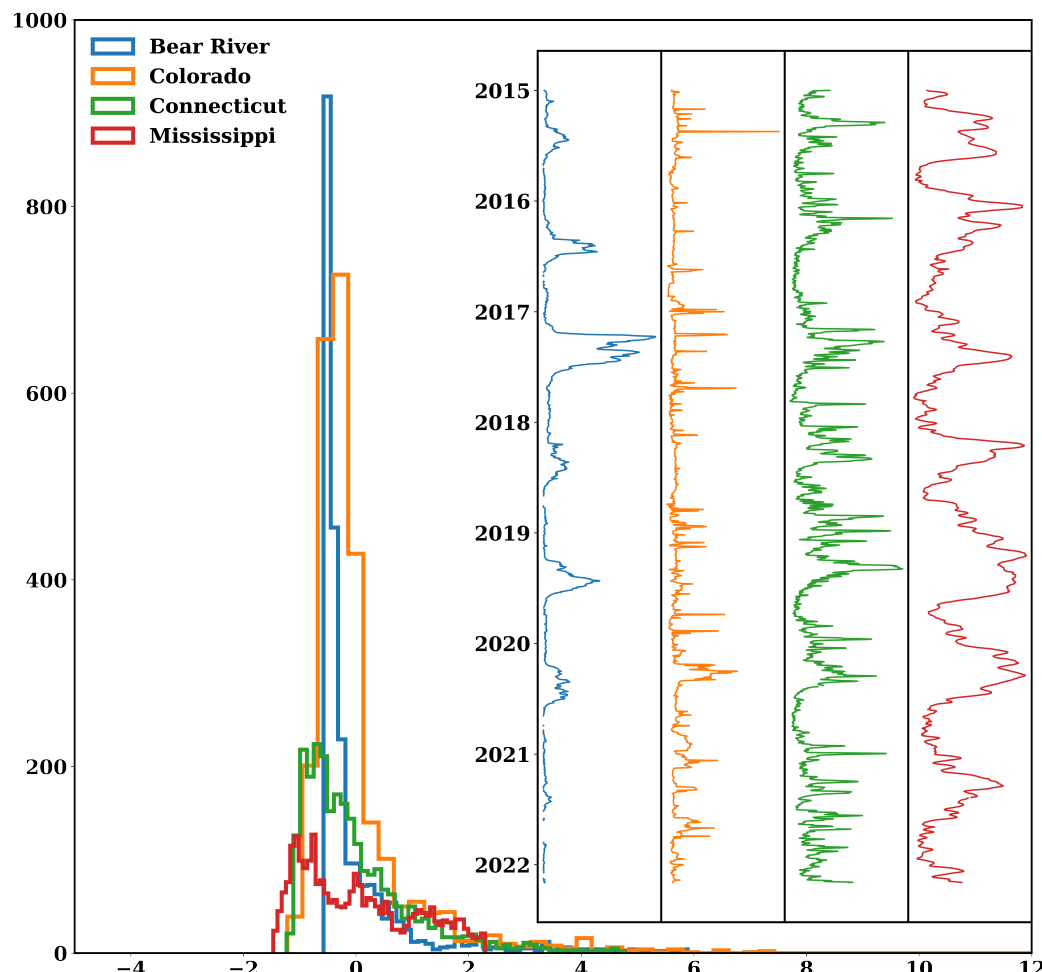


Figure 2. Strip chart and histogram plots of z-scored gauged streamflow observations.

We perform nine iterations of the configuration of 252 experiments. For each of the four basins, there are sixty-three experiments per iteration based on nine possible values of

lag and seven possible values of training and test data split, equating to 2268 individual runs of the same neural network. Each experiment either stops when the measurement of average NSE of the training dataset within an epoch equals 95% (bottom right, Figure 3) or the total number of epochs of back and forward propagation of the entire basin dataset reaches 100. The computations are constrained to a single node with two central processing units, a single NVIDIA GeForce RTX 2080 Ti graphical processing unit, and no more than 130 gigabytes of random access memory. Our platform is written in the python programming language and managed with the miniconda package manager. The total run time to compute the experiments was 83.0 h.

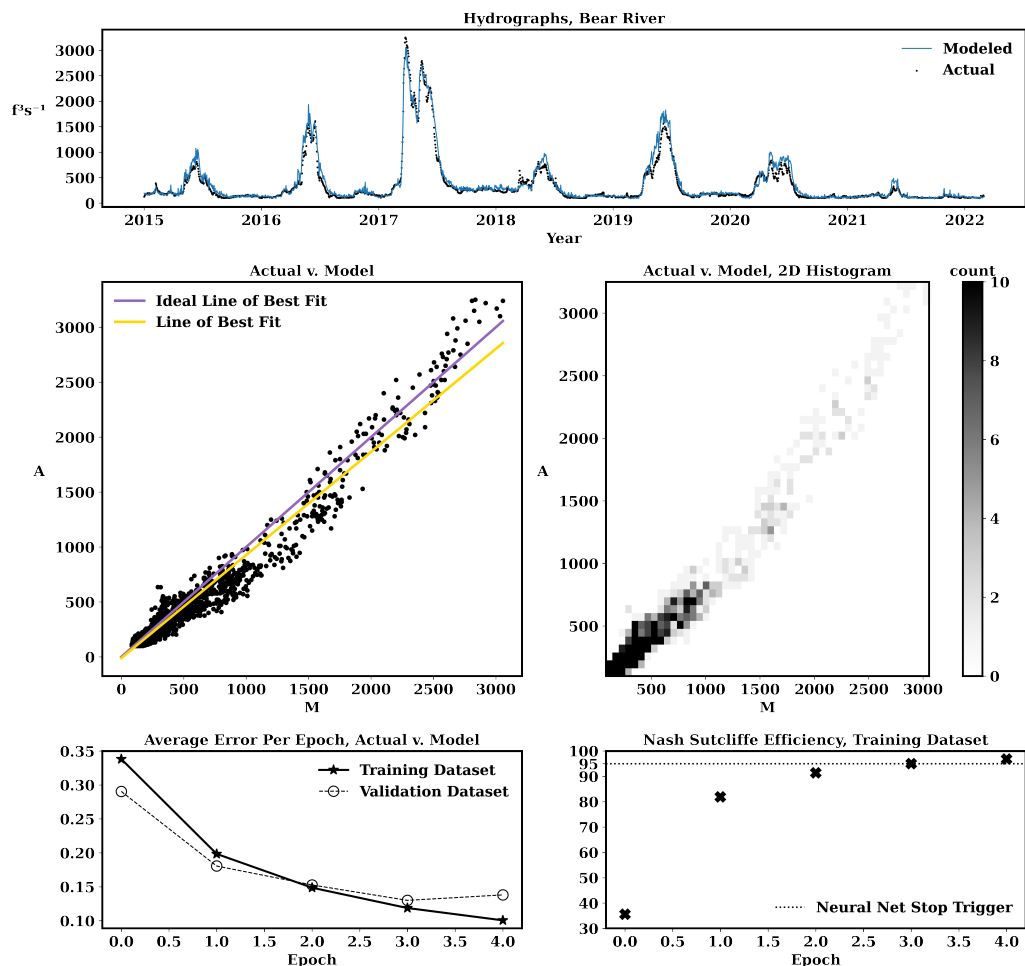


Figure 3. Neural network sample output.

3. Results

The hourly NLDAS model outputs of surface and subsurface flow are summed to daily accumulations over the time span of 1 January 2015 to 1 March 2022. This time series is 2617 days long and composed of two channel images. The channels are surface and subsurface flow measured in units of kilograms per square meter. These units are analogous to the weight of water in a location. The sample observation output from each basin capturing the flow behavior on 6 June 2021 is displayed in Figure 4. The effects of spatial resolution are apparent, as the Bear River and Connecticut River basins have pronounced rectangular edges due to their relatively small size. This pixelation effect is not present in the Mississippi River and Colorado River observations of lateral flow from the basin view at this constrained figure size.

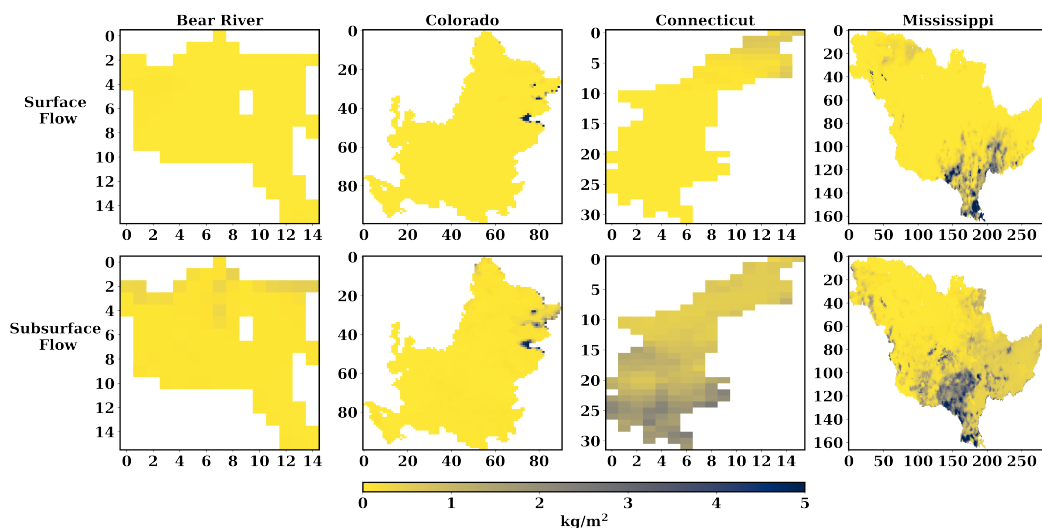


Figure 4. NLDAS daily surface and subsurface flows. Coordinates have been removed from these gridded images. The values of both axes refer to the relative horizontal and vertical count of pixels from the original located in the top left and are dimensionless.

Figure 3 shows a sample output from one configuration of the neural network. The topmost graph illustrates the time series of discharge measurements in cubic feet per second of the Bear River. This graph is rotated ninety degrees relative to its sibling hydrograph in Figure 2. There is a notable seasonality to this streamflow measurement of the Bear. Spring brings melting snowpack in the nearby mountainous terrain and subsequent increases in the neighboring river flows. The spring melting snow in 2021 appears more subdued than all other years observed. The Bear River drainage basin is located in between the Great Salt Lake and Yellowstone National Park in the Rocky Mountain region of the United States. The eponymously named river flows in a counterclockwise loop.

The second row plots each modeled observation in the time series against its respective actual measurement. On the left is a study of the model output ordered on the x-axis from low to high flows with the corresponding actual measurement on the y-axis. The right plot retains the same axis labels, but instead observes the spatial proximity of values. Darker points are more-commonly occurring ranges of flow. The left plot also contains two lines of best fit: the ideal or desired line found from the data and the actual line of fit as exists between the actual gauged streamflow and the neural network model output of streamflow from surface and subsurface flow.

The third and final row shows the epochal values during the neural network training process. On the left, the average error between the actual measurements and network output declines as the model goes through its iterations of propagate and backpropagate. Concomitant with the error vs. epoch is efficiency vs. epoch. As the error declines towards zero, the NSE measurement increases towards 100%. Here, the neural network was set to stop at an NSE value of 95%, which occurs in the sixth epoch.

4. Discussion

The results presented indicate a relatively favorable performance of the neural network architecture when transforming the surface and subsurface flow into a prediction of basin gauged streamflow; the kernel density estimates (KDE) in Figures 5 and 6 illustrate this point. We executed a total of more than 2200 experiments using the common architecture. We used two hydrological metrics: Kling–Gupta (KGE) and Nash–Sutcliffe (NSE) [40–43]. For each of these metrics, the peak resultant merit value of the 2268 experiments is greater than ninety percent with a standard deviation of less than 0.06. The results are tolerant to lagging the data beyond the residence time of water in the atmosphere [44,45]. This study presents a new simple framework that performs significantly better than the routing algorithm by the author of the input NLDAS input datasets. See [22] for a thorough

explanation. Their streamflow modeling results (with respect to NSE) are admitted to be less than desirable, and they encourage improvement in the NSE scores. Based on the performance here, we see the F2F methodology as a valid suitor for a follow-on dataset such as NLDAS-3.

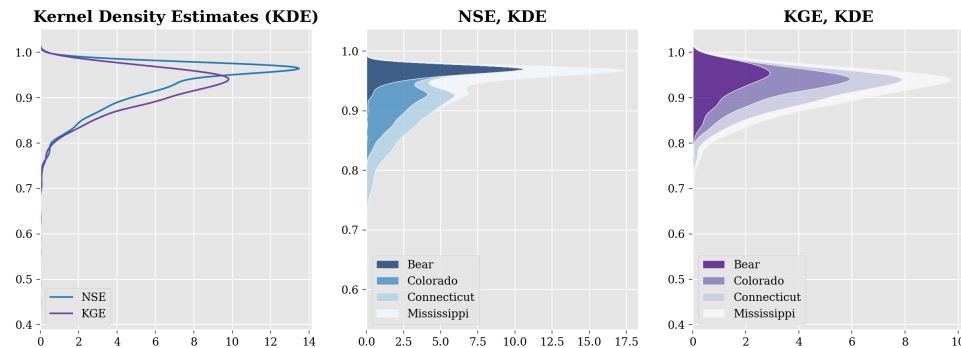


Figure 5. Kernel density estimates of the 2268 experiments. Left shows grand NSE and KGE.

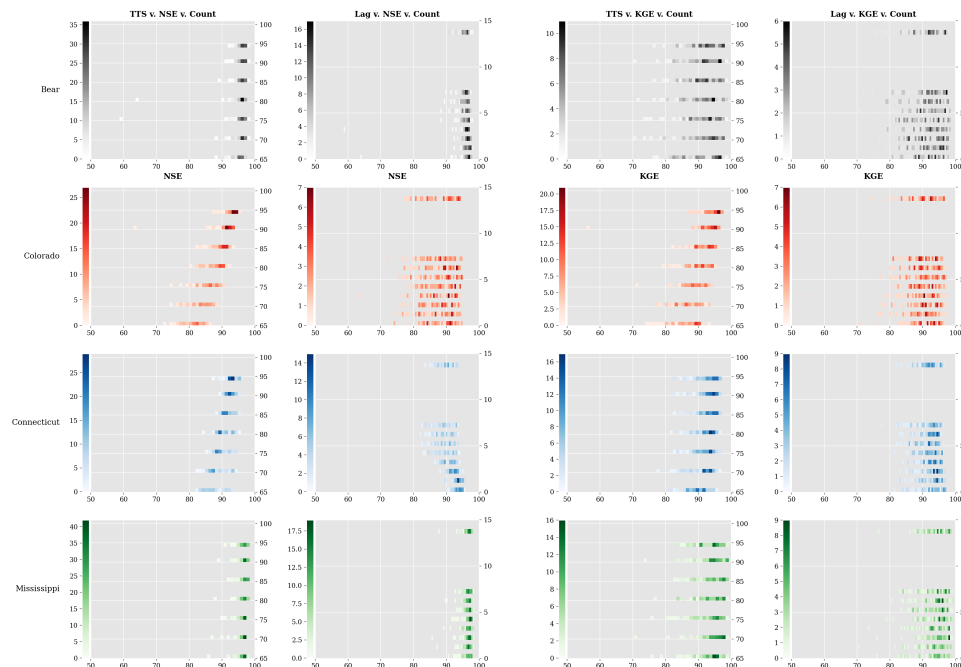


Figure 6. Three-dimensional merit plots, basin delineated by color. Intensity of color indicates higher frequency within bin range.

Others have observed the changing water quantity of the Mississippi. One study using NLDAS data focuses on a subsection of the Mississippi with a higher quantity of streamflow target sites [46]. Another group considers a different data system altogether for watershed modeling on the upper Mississippi basin [47]. Some groups suggest that NLDAS is too simplistic and decided to create their own blend. They take a much broader approach than the scope of the problem observed here [48]. The same is true for another study, which considers several different models and about 1000 small river basins [49]. Some use meteorological data as a predictor for electric outages, as seen in a study looking at Connecticut. They, too, use the Nash–Sutcliffe efficiency as a figure of merit [50] but approach the problem with a different lens. Their target is a smaller population and the risk of being without electric power.

This process can be expanded in different ways. Our study relies on the internal programming of NLDAS to compute the surface and subsurface flow. There is much uncertainty in these observations based on the natural heterogeneity of the land surface.

We do not look at the independent influence of any single forcing variable. Take snow, for example. In large mountain proximal basins such as those near the Rocky Mountains or Himalayan ranges, an accumulation of subzero-degree Celsius water in solid form provides a continuous upland buffer tank for the communities the river downland serves. As the relative presence of carbon dioxide increases and the land temperature responds in agreement, the duration and scale of snow melt and sea ice responds. It is challenging to equate with exact certainty how much solid water exists. To a degree, interpolating satellite data with gauged data is sufficient, but these apparatuses are challenging to maintain in cold temperatures or in places of very high altitude. One could elect to observe more individual locations as targets, therefore making the relationship no longer image-to-single-value at a given time, but instead image-to-image. There are studies that consider the impact of slow-moving oceanic and atmospheric abnormalities upon the hydrology of the land. Independent variables include the Madden–Julian oscillation [51], the El Niño–Southern Oscillation [52], and the Atlantic meridional overturning circulation [53].

While the NLDAS product used here is of a particular spatial fidelity, the Global Land Data Assimilation System is coarser in its resolution. It is beneficial to the scientific community to have a clearer picture of the meteorological forcing and environmental responses in the ocean, land, air, and mixed interfaces. One could use this framework to fuse the high-resolution NLDAS product with the global GLDAS product and evaluate the result according to one common set of metrics. The software could be packaged and ported to use with an already-existing embedded in situ mesh system to provide forecasting information. Instead, one might consider looking at a different time signature, such as seasonally decomposed but over several years. Instead, one might introduce higher-resolution localized water-quality data into the model. By tracking environmental statistical anomalies relative to other points in time and relative to the global community, municipal decision makers can clue into the trajectory of their land, their structures, and their constituents within. The choice to retreat is not to be approached lightly, but in some instances is becoming the necessary measure [54,55]. This intelligence can also be placed in the hands of consulting engineers to distribute in new and existing infrastructure. Logic is necessary to manage the assets of complex hydraulic systems (pumps, motors, chemical feed, aeration, dewatering, gates, valves), and digital twin systems are becoming fashionable.

In 2022, Pakistan and the United States were hit by massive floods that caused widespread devastation. In Pakistan, heavy monsoon rains led to flooding across the country, affecting millions of people and causing significant damage to infrastructure and property [56]. Similarly, in the United States, the Mississippi River experienced severe flooding due to heavy rainfall, causing extensive damage to homes, businesses, and farmland [57]. These events demonstrate the devastating impact that extreme water events can have on communities and the urgent need for improved water-management strategies.

Strong rotational winds cause hurricanes and cyclones, which carry bulk quantities of water. These catastrophes are notable for their brute strength and historically have caused the displacement of people, loss of lives, damage to infrastructure, and disruption of social and economic systems. One of the most notable wind-driven water-based disasters in recent years was Hurricane Harvey in 2017, which caused catastrophic flooding in Texas and Louisiana [58]. The storm resulted in over eighty fatalities and more than 125 billion in damages, making it one of the costliest natural disasters in US history. The intensity and frequency of hurricanes are expected to increase due to climate change, resulting in an increased risk of devastating floods and damage to coastal infrastructure [59]. Another significant event was Cyclone Idai, which hit Mozambique in 2019, causing widespread damage and loss of life. The storm resulted in over 1000 fatalities and an estimated economic loss of over USD2 billion. Cyclone Idai was one of the worst weather-related disasters to hit the southern hemisphere, highlighting the increasing vulnerability of developing countries to extreme weather events [60].

On the other end of the water-quantity-disaster spectrum, the 2017 Cape Town water crisis brought attention to the challenges of managing a sustained lack of renewable water

resources over a prolonged period of time. The city of Cape Town, South Africa faced an unprecedented drought that lasted for several years, leading to a severe water shortage. The crisis prompted the implementation of strict water-rationing measures and increased investment in water-conservation and -management strategies. This event highlighted the importance of proactive and adaptive water-management strategies in the face of changing environmental conditions [61].

The impacts of water-based disasters are not limited to the immediate physical damage they cause. These disasters can have long-lasting effects on the environment through vectors of water pollution and ecosystem degradation. For example, the 2011 Fukushima nuclear disaster in Japan led to the release of radioactive materials into the ocean, resulting in significant environmental damage. The incident, of course, had an impact on the surrounding marine ecosystem, with some species of fish still showing elevated levels of radiation years after the disaster [62,63].

Improving water-management strategies requires a multifaceted approach, including better monitoring systems, enhanced cooperation with the environment, and increased public awareness and participation. Effective water-management strategies should aim to balance the competing demands of human society and the natural environment while promoting the sustainable and equitable use of water resources. The opportunities to improve our monitoring systems are many; however, more people are needed in the conversation to consider how we might better cooperate with the environment.

Effective management and mitigation of water-based disasters require coordinated efforts from multiple stakeholders, including governments, non-governmental organizations, and the private sector. Such efforts include improving early warning systems, developing more resilient infrastructure, and promoting sustainable water-management practices. Early warning systems play a crucial role in preparing for and responding to water-based disasters. These systems can provide timely and accurate information to people in affected areas, enabling them to take necessary precautions and evacuate if necessary [64]. The development of more resilient infrastructure is also essential in mitigating the impact of water-based disasters [65]. For example, the use of green infrastructure, such as rain gardens and permeable pavement, can help to reduce the impact of flooding by slowing down the rate at which water enters the drainage system [66]. Additionally, the use of nature-based solutions, such as wetland restoration, can help to improve the overall resilience of ecosystems to climate change and extreme weather events [67].

Finally, it is crucial to recognize that the impacts of water-based disasters are not distributed equally. Vulnerable populations, such as those living in poverty or in marginalized communities, are often disproportionately affected by these events [68]. In addition, climate change is exacerbating the frequency and severity of water-based disasters, particularly in regions with already-limited resources and infrastructure [69]. Therefore, addressing the root causes of vulnerability and promoting equity in disaster management and response must be an integral part of efforts to mitigate the impacts of water-based disasters.

We find that the major limitation of Flux to Flow in this set of experiments is the small quantity of target outputs for a given basin. The Mississippi, for example, is an extremely large basin, and to boil the entirety of its existence down to a single gauged point is certainly an oversimplification of the basin's complexity. Future studies with Flux to Flow should improve the granularity of basin comprehension. This improved basin comprehension should both be literal in the words used to describe the basins, as well as more streamflow gauges. Furthermore, when we computed the efficiency values after each of the 2268 models was trained, we computed these values not just based on the test data but also including the training data. Certainly, this might allow for a positive biased result value because a large amount of training data has been factored into the performance of the system. Further studies should be harsher on the performance of Flux to Flow. More simultaneous target measurements are required, and only test data should be factored into the computation of network performance. We also looked at the derived fields of surface and subsurface flow that are computed via a host of meteorological forcings as

well as thoughtfully applied deterministic methods [22,70]. Because of this abstraction, it is possible that our work is carrying through biases created from oversimplification of the system that has been used to make our inputs.

It would be valuable to consider using more pure inputs and see if this provides a more robust performance. The factors that we see as potential next raw inputs are the consideration of terrain, land cover, and shifts in the land due to geophysical phenomena. The changing elevation of water is a crucial facet in the power of water. As such, there is a wide breadth of elevation data available and scientists focused on this aspect. Both elevation and land cover datasets are available with much finer resolution than the spatial scales considered here [71–73].

We constrained our research to a single computing node at a time. We are aware that this handicaps the scope of what can be computed in the experiments. However, we crafted the software so that it might be scaled to these larger and finer-resolution datasets. Furthermore, we only consider one neural network structure. It is possible that our system is more powerful than is necessary since our results seem to be mostly intolerant to lag or splitting of the data. Because of this, one way to distinguish F2F would be to consider its performance against other networks. There are no shortages of potential structures, but we think a logical next step would be to consider simpler structures such as the building block components of our dcrrnn architecture. Another avenue is to apply some of the newer, more complex structures. Some authors have already approached this topic in the Colorado basin [74]. Transformers are gaining much notoriety with the growth of large language models. It is less known that these same mechanisms can be applied to regressive tasks such as the one approached here and could prove to be a workhorse for climate modeling [75].

5. Conclusions

In this study, we introduce a fresh perspective to studying and understanding the water cycle with a learned representation using modern techniques and data systems. Our results show that a deep convolutional residual regressive neural network (dcrrnn) combined with water flux and gauged streamflow data can exhibit strong forecasting performance according to standard hydrological statistical figures of merit. We used the dcrrnn concept to develop a platform called Flux to Flow (F2F) and examined four major river basins across the United States. F2F outputs strong forecasting performances (Nash–Sutcliffe and Kling–Gupta efficiency above 90%) in most cases and at various time lags. Through the careful use of visuals and data management, this approach can provide a satisfactory performance for various locations, degrees of fidelity, time scales, and parameters of interest for the water resource and climate science community. Furthermore, we render the code in a form that is meant to be accompanied with the white paper. We believe that the hybridization of the literature with clearly written open-access software is the future of watershed modeling research (and research in general). We think this approach opens the door for new students who are interested in the water cycle, but who might be limited by 1. financial resources associated with black-box high-performing solutions or 2. their prior experience with the programming environment. We do not sacrifice modeling quality for simplicity of understanding and believe this is a unique facet of this research. We hope this work will spur others on in the quest for better prediction of the water cycle and conservation of the global ecosystem.

Author Contributions: Writing—data analysis and original draft preparation, A.L.; writing—review and editing, A.L., T.B. and A.S.A.; review; A.H. and S.M.P.; supervision, A.S.A.; funding acquisition, A.L. and A.S.A. All authors have read and agreed to the published version of the manuscript.

Funding: This research was supported, in part, by a Fellowship from the National Space Grant College and Fellowship Program—Opportunities in NASA STEM-NNH19ZHA001C.

Institutional Review Board Statement: Not applicable.

Data Availability Statement: Scripts are available at <https://github.com/albertlarson/f2f> (accessed on 30 March 2023).

Acknowledgments: The authors thank to the University of Rhode Island Research Computing Services and the Massachusetts Green High Performing Computing Center for use and support of the UNITY cluster.

Conflicts of Interest: The authors declare no conflict of interest.

Abbreviations

The following abbreviations are used in this manuscript:

dcrnn	deep convolutional residual regressive neural network
F2F	Flux to Flow
NASA	National Aeronautics and Space Administration
GLDAS	Global Land Data Assimilation System
NLDAS	National Land Data Assimilation System
USGS	United States Geological Survey
kg/m ²	kilograms per square meter
ft ³ /s	cubic feet per second
A	actual gauged in the river measurement
M	modeled measurement via neural network
NSE	Nash–Sutcliffe efficiency
KGE	Kling–Gupta efficiency
KDE	kernel density estimate
TTS	training–test split

References

1. Stott, P. How climate change affects extreme weather events. *Science* **2016**, *352*, 1517–1518. [[CrossRef](#)] [[PubMed](#)]
2. Qin, Y.; Abatzoglou, J.T.; Siebert, S.; Huning, L.S.; AghaKouchak, A.; Mankin, J.S.; Hong, C.; Tong, D.; Davis, S.J.; Mueller, N.D. Agricultural risks from changing snowmelt. *Nat. Clim. Chang.* **2020**, *10*, 459–465. [[CrossRef](#)]
3. Min, C.; Yang, Q.; Chen, D.; Yang, Y.; Zhou, X.; Shu, Q.; Liu, J. The emerging Arctic shipping corridors. *Geophys. Res. Lett.* **2022**, *45*, e2022GL099157. [[CrossRef](#)]
4. Tebaldi, C.; Ransinghe, R.; Voudoukas, M.; Rasmussen, D.; Vega-Westhoff, B.; Kirezci, E.; Kopp, R.E.; Srivastava, R.; Mentaschi, L. Extreme sea levels at different global warming levels. *Nat. Clim. Chang.* **2021**, *11*, 746–751. [[CrossRef](#)]
5. Sévellec, F.; Fedorov, A.V.; Liu, W. Arctic sea-ice decline weakens the Atlantic meridional overturning circulation. *Nat. Clim. Chang.* **2017**, *7*, 604–610. [[CrossRef](#)]
6. Karl, T.R.; Nicholls, N.; Gregory, J. The coming climate. *Sci. Am.* **1997**, *276*, 78–83. [[CrossRef](#)]
7. Underwood, E. Models predict longer, deeper US droughts. *Science* **2015**, *347*, 707. [[CrossRef](#)]
8. Milly, P.C.D.; Wetherald, R.T.; Dunne, K.; Delworth, T.L. Increasing risk of great floods in a changing climate. *Nature* **2002**, *415*, 514–517. [[CrossRef](#)]
9. Hirabayashi, Y.; Mahendran, R.; Koitala, S.; Konoshima, L.; Yamazaki, D.; Watanabe, S.; Kim, H.; Kanae, S. Global flood risk under climate change. *Nat. Clim. Chang.* **2013**, *3*, 816–821. [[CrossRef](#)]
10. Parmesan, C.; Root, T.L.; Willig, M.R. Impacts of extreme weather and climate on terrestrial biota. *Bull. Am. Meteorol. Soc.* **2000**, *81*, 443–450. [[CrossRef](#)]
11. Gleick, P.H.; Cooley, H. Freshwater Scarcity. *Annu. Rev. Environ. Resour.* **2021**, *46*, 319–348. [[CrossRef](#)]
12. Crisp, N.H.; Roberts, P.C.; Livadiotti, S.; Oiko, V.T.A.; Edmondson, S.; Haigh, S.; Huyton, C.; Simpetru, L.; Smith, K.; Worrall, S.; et al. The benefits of very low earth orbit for earth observation missions. *Prog. Aerosp. Sci.* **2020**, *117*, 100619. [[CrossRef](#)]
13. Minzu, V.; Riahi, S.; Rusu, E. Optimal control of an ultraviolet water disinfection system. *Appl. Sci.* **2021**, *11*, 2638. [[CrossRef](#)]
14. Horton, P.; Schaeffli, B.; Kauzlaric, M. Why do we have so many different hydrological models? A review based on the case of Switzerland. *Wiley Interdiscip. Rev. Water* **2022**, *9*, e1574. [[CrossRef](#)]
15. Abbaspour, K.C.; Yang, J.; Maximov, I.; Siber, R.; Bogner, K.; Mieleitner, J.; Zobrist, J.; Srinivasan, R. Modelling hydrology and water quality in the pre-alpine/alpine Thur watershed using SWAT. *J. Hydrol.* **2007**, *333*, 413–430. [[CrossRef](#)]
16. Wang, Y.; Jiang, R.; Xie, J.; Zhao, Y.; Yan, D.; Yang, S. Soil and water assessment tool (SWAT) model: A systemic review. *J. Coast. Res.* **2019**, *93*, 22–30. [[CrossRef](#)]
17. Beven, K.J.; Buytaert, W.; Smith, L.A.; Westerberg, I.K.; McMillan, H.K. A decade of Predictions in Ungauged Basins (PUB)—A review. *Hydrol. Sci. J.* **2013**, *58*, 1198–1255.
18. Kiehl, J.T. Twentieth century climate model response and climate sensitivity. *Geophys. Res. Lett.* **2007**, *34*, L22710. [[CrossRef](#)]

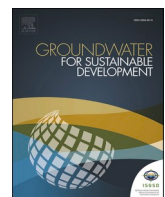
19. Vano, J.A.; Das, T.; Tague, C.; Padowski, J.; Udall, B.; Bart, R.; Klos, P.Z. Hydrologic implications of dynamical and statistical approaches to downscaling climate model outputs. *Clim. Chang.* **2013**, *119*, 519–539.
20. Haidvogel, D.B.; Arango, H.G.; Hedstrom, K.S.; Beckmann, A.; Malanotte-Rizzoli, P.; Shchepetkin, A.F. Model evaluation experiments in the North Atlantic Basin: Simulations in nonlinear terrain-following coordinates. *Dyn. Atmos. Ocean.* **2008**, *44*, 28–48. [CrossRef]
21. Marshall, J.; Adcroft, A.; Hill, C.; Perelman, L.; Heisey, C. A finite-volume, incompressible Navier Stokes model for studies of the ocean on parallel computers. *J. Geophys. Res. Ocean.* **1997**, *102*, 5753–5766. [CrossRef]
22. Xia, Y.; Mitchell, K.; Ek, M.; Sheffield, J.; Cosgrove, B.; Wood, E.; Luo, L.; Alonge, C.; Wei, H.; Meng, J.; et al. Continental-scale water and energy flux analysis and validation for the North American Land Data Assimilation System project phase 2 (NLDAS-2): 1. Intercomparison and application of model products. *J. Geophys. Res. Atmos.* **2012**, *117*, D03109. [CrossRef]
23. Liang, X.; Lettenmaier, D.P.; Wood, E.F.; Burges, S.J. A simple hydrologically based model of land surface water and energy fluxes for general circulation models. *J. Geophys. Res. Atmos.* **1994**, *99*, 14415–14428. [CrossRef]
24. Ries, K.G. The national water information system: A United States government water data infrastructure. *Int. J. River Basin Manag.* **2015**, *13*, 289–298.
25. Mueller, D.K.; Wagner, R.J.; Nystrom, E.A. Overview of the United States Geological Survey National Water Information System database. *J. Water Resour. Plan. Manag.* **2016**, *142*, 05016004.
26. Stewart, D.W.; Caldwell, R.R.; Hunt, R.J.; Viger, R.J. The US Geological Survey’s Water Availability and Use Science Program: Overview and selected research activities. *US Geol. Surv. Fact Sheet* **2018**, *2018*, 1–6.
27. Benson, M.A.; Carter, J.M.; Ritzman, R.A.; Landers, M.N. US Geological Survey stream-gaging program: Overview and highlights, 1879–2007. *US Geol. Surv. Circ.* **2009**, *1331*, 1–60.
28. Hirsch, R.M.; De Cicco, L.A. USGS streamgages and US Environmental Protection Agency water quality monitoring: A successful partnership. *Environ. Monit. Assess.* **2010**, *171*, 21–27.
29. Karhunen, J.; Oja, E.; Wang, L.; Vigario, R.; Joutsensalo, J. A class of neural networks for independent component analysis. *IEEE Trans. Neural Netw.* **1997**, *8*, 486–504. [CrossRef]
30. Chen, Z.; Bei, Y.; Rudin, C. Concept whitening for interpretable image recognition. *Nat. Mach. Intell.* **2020**, *2*, 772–782. [CrossRef]
31. He, K.; Zhang, X.; Ren, S.; Sun, J. Deep residual learning for image recognition. In Proceedings of the IEEE Conference on Computer Vision and Pattern Recognition, Las Vegas, NV, USA, 27–30 June 2016; pp. 770–778.
32. Weiss, K.; Khoshgoftaar, T.M.; Wang, D. A survey of transfer learning. *J. Big Data* **2016**, *3*, 9. [CrossRef]
33. David, C.H.; Maidment, D.R.; Niu, G.Y.; Yang, Z.L.; Habets, F.; Eijkhout, V. River network routing on the NHDPlus dataset. *J. Hydrometeorol.* **2011**, *12*, 913–934. [CrossRef]
34. PyTorch. PyTorch: Deep Learning with PyTorch. Available online: https://pytorch.org/tutorials/beginner/deep_learning_60_min_blitz.html (accessed on 30 March 2023).
35. Rawat, W.; Wang, Z. Deep convolutional neural networks for image classification: A comprehensive review. *Neural Comput.* **2017**, *29*, 2352–2449. [CrossRef] [PubMed]
36. Agarap, A.F. Deep learning using rectified linear units (relu). *arXiv* **2018**, arXiv:1803.08375.
37. Ioffe, S.; Szegedy, C. Batch normalization: Accelerating deep network training by reducing internal covariate shift. In *International Conference on Machine Learning*; PMLR: London, UK, 2015; pp. 448–456.
38. Amari, S.i. Backpropagation and stochastic gradient descent method. *Neurocomputing* **1993**, *5*, 185–196. [CrossRef]
39. Kingma, D.P.; Ba, J. Adam: A method for stochastic optimization. *arXiv* **2014**, arXiv:1412.6980.
40. Nash, J.E.; Sutcliffe, J.V. River flow forecasting through conceptual models part I—A discussion of principles. *J. Hydrol.* **1970**, *10*, 282–290. [CrossRef]
41. Gupta, H.; Kling, H.; Yilmaz, K.; Martinez, G. Decomposition of the mean squared error and NSE performance criteria: Implications for improving hydrological modelling. *J. Hydrol.* **2009**, *377*, 80–91. [CrossRef]
42. Gupta, H.; Kling, H. On typical range, sensitivity, and normalization of Mean Squared Error and Nash-Sutcliffe Efficiency type metrics. *Water Resour. Res.* **2011**, *47*, W10601. [CrossRef]
43. Knoben, W.J.; Freer, J.E.; Woods, R.A. Inherent benchmark or not? Comparing Nash–Sutcliffe and Kling–Gupta efficiency scores. *Hydrol. Earth Syst. Sci.* **2019**, *23*, 4323–4331. [CrossRef]
44. Van Der Ent, R.J.; Tuinenburg, O.A. The residence time of water in the atmosphere revisited. *Hydrol. Earth Syst. Sci.* **2017**, *21*, 779–790. [CrossRef]
45. Gimeno, L.; Eiras-Barca, J.; Durán-Quesada, A.M.; Dominguez, F.; van der Ent, R.; Sodemann, H.; Sánchez-Murillo, R.; Nieto, R.; Kirchner, J.W. The residence time of water vapour in the atmosphere. *Nat. Rev. Earth Environ.* **2021**, *2*, 558–569. [CrossRef]
46. Qi, J.; Wang, Q.; Zhang, X. On the use of NLDAS2 weather data for hydrologic modeling in the Upper Mississippi River Basin. *Water* **2019**, *11*, 960. [CrossRef]
47. Chen, M.; Cui, Y.; Gassman, P.W.; Srinivasan, R. Effect of watershed delineation and climate datasets density on runoff predictions for the Upper Mississippi River Basin using SWAT within HAWQS. *Water* **2021**, *13*, 422. [CrossRef]
48. Tran, H.; Zhang, J.; O’Neill, M.M.; Ryken, A.; Condon, L.E.; Maxwell, R.M. A hydrological simulation dataset of the Upper Colorado River Basin from 1983 to 2019. *Sci. Data* **2022**, *9*, 16. [CrossRef]
49. Cai, X.; Yang, Z.L.; Xia, Y.; Huang, M.; Wei, H.; Leung, L.R.; Ek, M.B. Assessment of simulated water balance from Noah, Noah-MP, CLM, and VIC over CONUS using the NLDAS test bed. *J. Geophys. Res. Atmos.* **2014**, *119*, 13–751. [CrossRef]

50. Yang, F.; Cerrai, D.; Anagnostou, E.N. The effect of lead-time weather forecast uncertainty on outage prediction modeling. *Forecasting* **2021**, *3*, 501–516. [CrossRef]
51. Jiang, X.; Adames, Á.F.; Kim, D.; Maloney, E.D.; Lin, H.; Kim, H.; Zhang, C.; DeMott, C.A.; Klingaman, N.P. Fifty years of research on the Madden-Julian Oscillation: Recent progress, challenges, and perspectives. *J. Geophys. Res. Atmos.* **2020**, *125*, e2019JD030911. [CrossRef]
52. Hu, D.; Wu, L.; Cai, W.; Gupta, A.S.; Ganachaud, A.; Qiu, B.; Gordon, A.L.; Lin, X.; Chen, Z.; Hu, S.; et al. Pacific western boundary currents and their roles in climate. *Nature* **2015**, *522*, 299–308. [CrossRef]
53. Ionita, M.; Nagavciuc, V.; Scholz, P.; Dima, M. Long-term drought intensification over Europe driven by the weakening trend of the Atlantic Meridional Overturning Circulation. *J. Hydrol. Reg. Stud.* **2022**, *42*, 101176. [CrossRef]
54. Siders, A.R. Social justice implications of US managed retreat buyout programs. *Clim. Chang.* **2019**, *152*, 239–257. [CrossRef]
55. Hino, M.; Field, C.B.; Mach, K.J. Managed retreat as a response to natural hazard risk. *Nat. Clim. Chang.* **2017**, *7*, 364–370. [CrossRef]
56. GulfNews. Death Toll from Pakistan Floods Reaches 25. *Gulf News*, 5 September 2022.
57. CBS. Flooding across Mississippi Amid Heavy Rainfall. *CBS News*, 29 August 2022.
58. Blake, E.S.; Gibney, E.J.; Center, N.H. Hurricane Harvey: 17–31 August 2017. *Mon. Weather. Rev.* **2018**, *146*, 3605–3609. [CrossRef]
59. Elsner, J.B.; Basu, S.; Fragomeni, M.V. Projected Atlantic hurricane surge threat from rising temperatures. *Environ. Res. Lett.* **2020**, *15*, 014014. [CrossRef]
60. Charrua, A.B.; Padmanaban, R.; Cabral, P.; Bandeira, S.; Romeiras, M.M. Impacts of the tropical cyclone idai in mozambique: A multi-temporal landsat satellite imagery analysis. *Remote Sens.* **2021**, *13*, 201. [CrossRef]
61. Parks, R.; McLaren, M.; Toumi, R.; Rivett, U. *Experiences and Lessons in Managing Water from Cape Town*; Grantham Institute Briefing Paper No. 29; Imperial College London: London, UK, 2019; pp. 1–20.
62. Zhao, C.; Wang, G.; Zhang, M.; Wang, G.; de With, G.; Bezhnar, R.; Maderich, V.; Xia, C.; Zhao, B.; Jung, K.T.; et al. Transport and dispersion of tritium from the radioactive water of the Fukushima Daiichi nuclear plant. *Mar. Pollut. Bull.* **2021**, *169*, 112515. [CrossRef]
63. Machida, M.; Yamaguchi, T.; Okuda, K.; et al. Current and historical cesium distribution in sediments in Fukushima coastal estuaries: Impact of a mega-typhoon on the remobilization and accumulation of radiocesium. *J. Environ. Radioact.* **2018**, *189*, 109–116. [CrossRef]
64. Ghosh, S.; Islam, M.R.; Danish, M.S.S. A review of early warning systems for urban flood management. *J. Hydrol.* **2017**, *548*, 672–691. [CrossRef]
65. Goodwill, J.E.; Ray, P.; Nock, D.; Miller, C.M. Emerging investigator series: Moving beyond resilience by considering antifragility in potable water systems. *Environ. Sci. Water Res. Technol.* **2022**, *8*, 8–21. [CrossRef]
66. Vogel, J.; Åkesson, A.; Bohnenstengel, K.; et al. Evaluating the impact of blue-green infrastructure on urban flooding in southeast Norway using hydrodynamic modelling. *Sustainability* **2019**, *11*, 335. [CrossRef]
67. CBD. Convention on Biological Diversity-Nature-Based Solutions. 2019. Available online: <https://www.cbd.int> (accessed on 11 April 2023).
68. Ebi, K.L.; Ford, J.D. Inequalities in heat-related mortality in a warming world: The role of adaptive capacity. *Curr. Epidemiol. Rep.* **2019**, *6*, 61–69. [CrossRef]
69. Masson-Delmotte, V.; Zhai, P.; Pörtner, H.O.; Roberts, D.; Skea, J.; Shukla, P.R.; Pirani, A.; Moufouma-Okia, W.; Péan, C.; Pidcock, R.; et al. Global warming of 1.5 C. *IPCC Spec. Rep. Impacts Glob. Warm.* **2018**, *1*, 43–50.
70. Xia, Y.; Ek, M.; Wei, H.; Meng, J. Comparative analysis of relationships between NLDAS-2 forcings and model outputs. *Hydrol. Process* **2012**, *26*, 467–474. [CrossRef]
71. East, A.E.; Stevens, A.W.; Ritchie, A.C.; Barnard, P.L.; Campbell-Swarzenski, P.; Collins, B.D.; Conaway, C.H. A regime shift in sediment export from a coastal watershed during a record wet winter, California: Implications for landscape response to hydroclimatic extremes. *Earth Surf. Process. Landf.* **2018**, *43*, 2562–2577. [CrossRef]
72. Brown, C.F.; Brumby, S.P.; Guzder-Williams, B.; Birch, T.; Hyde, S.B.; Mazzariello, J.; Czerwinski, W.; Pasquarella, V.J.; Haertel, R.; Ilyushchenko, S.; et al. Dynamic World, Near real-time global 10 m land use land cover mapping. *Sci. Data* **2022**, *9*, 251. [CrossRef]
73. Derakhshani, R.; Zaresefat, M.; Nikpeyman, V.; GhasemiNejad, A.; Shafeibafti, S.; Rashidi, A.; Nemati, M.; Raoof, A. Machine Learning-Based Assessment of Watershed Morphometry in Makran. *Land* **2023**, *12*, 776. [CrossRef]
74. Hosseinzadeh, P.; Nassar, A.; Boubrahimi, S.F.; Hamdi, S.M. ML-Based Streamflow Prediction in the Upper Colorado River Basin Using Climate Variables Time Series Data. *Hydrology* **2023**, *10*, 29. [CrossRef]
75. Khan, S.; Naseer, M.; Hayat, M.; Zamir, S.W.; Khan, F.S.; Shah, M. Transformers in vision: A survey. *ACM Comput. Surv. (CSUR)* **2022**, *54*, 1–41. [CrossRef]

Disclaimer/Publisher’s Note: The statements, opinions and data contained in all publications are solely those of the individual author(s) and contributor(s) and not of MDPI and/or the editor(s). MDPI and/or the editor(s) disclaim responsibility for any injury to people or property resulting from any ideas, methods, instructions or products referred to in the content.



Groundwater for Sustainable Development

journal homepage: www.elsevier.com/locate/gsd

Research paper

Quantifying groundwater depletion in Arabian Peninsula transboundary aquifer systems: Understanding natural and anthropogenic drivers

Mohammed O. Altayyar^a, Shoaib Ali^b, Albert E. Larson^c, Thomas Boving^{a,d}, Leon Thiem^a, Ali S. Akanda^{a,*}

^a Department of Civil and Environmental Engineering, University of Rhode Island, Kingston, RI, 02881, USA

^b Water Conservancy and Civil Engineering College, Northeast Agricultural University, Harbin, China

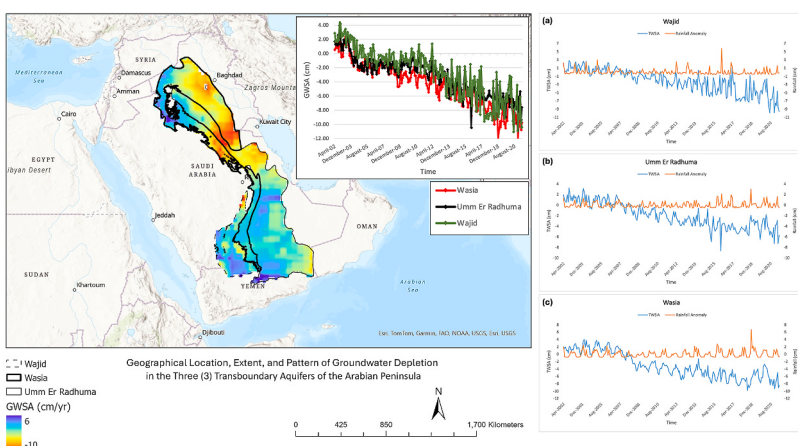
^c Department of Earth, Environmental and Planetary Sciences, Brown University, Providence, RI, 02912, USA

^d Department of Geosciences, University of Rhode Island, Kingston, RI, 02881, USA

HIGHLIGHTS

- Transboundary aquifers in the Arabian Peninsula show major groundwater depletion.
- Highest decline is seen in central and north central Saudi Arabia and border regions.
- Remote Sensing-based monitoring can help efficient management of regional aquifers.

GRAPHICAL ABSTRACT



ARTICLE INFO

Keywords:
Arabian Peninsula
Groundwater depletion
Transboundary aquifers
Groundwater treaties
GRACE
GRACE-FO

ABSTRACT

Groundwater is the primary source of freshwater for domestic, agricultural, and industrial usage in the Arabian Peninsula countries. It is increasingly becoming a limited resource due to human activities leading to excessive depletion and contamination. Thus, sustainable management of groundwater resources in this region is critical. The groundwater in the Arabian Peninsula countries is primarily found in transboundary systems such as the Wajid, Umm Er Radhuma, and Wasia Aquifers shared between Saudi Arabia, Iraq, Syria, Yemen, and Oman. These systems have no groundwater-sharing agreements, which leads to a lack of data sharing, unsustainable and uncoordinated development, rapid water depletion, water quality deterioration, and land subsidence. This study examines the Wajid, Umm Er Radhuma, and Wasia aquifer systems from April 2002 to May 2021 by analyzing monthly gravity field solutions from GRACE and GRACE-FO satellite data, other remote sensing observations, information from the Global Land Data Assimilation System (GLDAS), as well as field data to determine how

* Corresponding author.

E-mail address: akanda@uri.edu (A.S. Akanda).

regional water resources are changing over time and to identify the factors that influence these resources. The sharp decline in Total Water Storage Anomalies (TWSA) and the Groundwater Storage Anomalies (GWSA) across all three systems is caused by a combination of climatic and human factors. The observed decline in Total Water Storage can be partly attributed to a decrease in regional rainfall, whereas the depletion of Groundwater Storage has a strong correlation with the rise in groundwater extraction for irrigation purposes in the 2010s. The recent rise is groundwater depletion in specific areas of central Saudi Arabia may be attributed to agricultural irrigation and rapid urban development. The results are insightful for monitoring water storage in management plans and decision-making processes to preserve and efficiently use groundwater resources.

1. Introduction

The world is going through unprecedented levels of water crisis in recent years, which influences every facet of our society, such as the environment, economy, energy, food, and health. Moreover, climatic and anthropogenic changes due to human activities and development play a significant role in ongoing water shortages, particularly in developing countries (Liuzzo et al., 2015; Moghim, 2020).

Water scarcity is especially severe and acutely felt in the vast dry regions across the Middle East and North Africa (MENA) region (Jasechko et al., 2024). The Arabian Peninsula countries are arid and semi-arid regions experiencing escalating populations and rapid growth. Groundwater is this region's primary source of freshwater, and precipitation acts as the recharging source (Fallatah et al., 2017; Kinzelbach et al., 2002; Scanlon et al., 2002; Sultan et al., 2008). Increased agricultural development and excessive groundwater extraction have caused a sharp decline in groundwater storage over the central and northern Arabian Gulf (Othman et al., 2018).

Kingdom of Saudi Arabia (KSA) is the largest country in this region, facing inveterate water insecurity. KSA's population increased almost 9 times between 1960 and 2021, and currently stands over 34 million (GASTAT, 2022). This rapid growth resulted in a significant increase in freshwater use. For instance, annual freshwater resources consumption in Saudi Arabia was estimated at $24.8 \times 10^9 m^3$ in 2015, but is anticipated to grow to $29.5 \times 10^9 m^3$ by 2050 (Fallatah et al., 2019; MEWA, 2021).

Also, most of the groundwater in the Arabian Peninsula is stored in transboundary aquifer systems (TBS) such as the Wajid, Umm Er Radhuma, and Wasia aquifers shared between Saudi Arabia, Yemen, Iraq, Syria, and Oman. As these countries do not have any groundwater sharing treaties, it leads to a lack of sharing data, unsustainable and uncoordinated development, increased water depletion, water quality and quantity, and land subsidence issues (Abdulrazzak et al., 2020; Mechlem, 2011).

The primary technologies used for artificial aquifer recharge in arid and semiarid regions include recharge basins, floodwater spreading systems, injection wells or recharge wells, and recharge dams (Mohammadzadeh-Habili and Khalili, 2020). Among the 213 dams distributed over KSA (Table 1), only two are located inside the aquifer

area, and are expected to serve as recharge dams. One is shown in the Wasia Aquifer region, named the Altamriyah dam, an earthen type situated in Riyadh province; the other is in the Umm Er Radhuma region, called the Safar dam, which is an earthen type located in Eastern province. Three dams on Wasia's border areas (4~15 km) are also considered to be recharge dams named Boudha (rock fill type), Haer Jouy, and Asheera dams (earthen type). Similarly, five dams on Wajid's borders (4~32 km) named Alhawatih, Hilwah, Lassad, Alhareeq dams (earthen type), and Alghaeel dams (concrete type), are contributing towards recharging the aquifer (MEWA, 2021).

Recently, satellite remote sensing has significantly improved our capability to monitor large scale changes in water resources of arid regions (Fallatah et al., 2017, 2019; Famiglietti, 2014; Famiglietti et al., 2013). For instance, the Gravity Recovery and Climate Experiment GRACE is a joint project between NASA and German Aerospace Centre launched in March 2002. GRACE has produced monthly gravity field solutions from April 2002 to June 2017, and GRACE-FO has continued that record from June 2018 onwards (<https://www.gfz-potsdam.de/en/grace>). The gravity solutions can be used to deduce the anomalies in total water mass, involving all water cycle components, over a specified geographic region (spatial resolution $0.25^\circ \times 0.25^\circ$). In addition, the Global Land Data Assimilation System (GLDAS), which incorporates satellite and ground-based observational data products can be used for advanced land surface modeling and data assimilation. The remotely sensed data drives four land surface models: Noah, Mosaic, Community Land Model (CLM), and the Variable Infiltration Capacity model (VIC) (Rodell et al., 2004; Rui and Beaudoing, 2020). Combining the total water storage information from GRACE and GRACE-FO observations and hydroclimatic variables from GLDAS simulations now provide us an improved and more accurate method of estimating the time series of water cycle components of arid region watersheds and aquifer systems, where data are not easily available.

Using such an approach, this study quantifies the spatiotemporal variations of water resources available in the transboundary aquifer systems of the Arabian Peninsula region. It also analyzed the evolving water demand in Wajid, Umm er Radhuma, and Wasia aquifer systems over the last two decades by combining earth observations, and climate and land surface components from GRACE, GRACE-FO, and GLDAS, respectively. The use of a satellite remote sensing-based approach allows us to monitor large scale changes in water resources over the vast arid and semi-arid landscape of the Middle East, where local water demand and withdrawal data are hard to obtain. The research objectives of this study are: 1) Quantify the rate of terrestrial water storage and groundwater usage and depletion, 2) Corroborate the finding of the remote sensing observations with land surface modeling results and ground observations, 3) Identify the climatic and anthropogenic factors driving water demand growth, groundwater depletion, and environmental changes in this region. Results show spatiotemporal changes in water storages, depletion, and the necessity of tracking groundwater resource changes for decision-makers and stakeholders to preserve the water resources and reduce their depletion rates.

Table 1
Dams in KSA.

KSA Province	Dams	Type
Riyadh	55	Concrete, Earthen, and Rock-fill
Mecca	22	Concrete, Earthen, Rock-fill, and underground
Eastern	1	Earthen
Almadinah	17	Concrete, Earthen, and Rock-fill
Bahah	26	Concrete, Earthen, and Rock-fill
Aljawf	2	Earthen
Northern Borders	0	
Alqassim	4	Concrete, Earthen
Hail	18	Concrete, Earthen
Asir	58	Concrete, Earthen, and Rock-fill
Jizan	4	Concrete, Earthen
Tabuk	0	
Najran	6	Concrete, Earthen
Total	213	

2. Data and methods

2.1. Study area

The climate of the Arabian Peninsula is characterized by low precipitation and high annual temperature (Fallatah et al., 2017). The central part of the peninsula is extremely hot in summer but relatively cold in winter, particularly at night and early morning. Northern and southern part of the Arabian Peninsula experience freezing temperatures in winter and sometimes snow in the north (Edgell, 2006). Geographically, the Arabian Peninsula can be classified into desert islands, coastal plains, salt flats, deltas, sand deserts, plateau, mountains, and scrap mountain regions (Brown et al., 1989; Edgell, 2006; Vegetation of the Arabian Peninsula," 1998). This region has experienced significant changes in its climate over the past decades, with rising temperatures and shifting weather patterns (Almazroui et al., 2020). It also experienced a steady increase in average temperatures, resulting in more frequent and intense heat waves, due to both natural climate variability and human-induced global warming.

The study region covers the three most significant transboundary aquifers in the Arabian Peninsula (AP), the Wajid, Umm Er Radhuma, and Wasia aquifer systems illustrated in Fig. 1. The Wajid aquifer is in the southern region of the AP, shared by Saudi Arabia and Yemen, and covers approximately a total area of 124,837 Km². The Umm er Radhuma aquifer is one of the most significant aquifers in the Arabian

Peninsula, which extends from northern to southern AP, and covers approximately 463,416 Km²; the Wasia aquifer, extending from the northern to southern part of the AP, is one of the most fertile groundwater sources in Saudi Arabia, providing freshwater resources to the capital city Riyadh (Alfaifi et al., 2017; Khogali et al., 2020). Its area is approximately 352,622 Km² (MEWA, 2021).

The Wajid aquifer serves more than 13 million people including 90% living in KSA, and 10% in Yemen, while the Umm Er Radhuma aquifer serves more than 20 million people including 73% living in KSA, 20% in Iraq, 5% in Yemen, and 2% in Oman. In addition, the Wasia aquifer serves more than 34 million people including 52% living in KSA, 41% in Iraq, 3% in Yemen, and 4% in Syria (Table 2) (GASTAT, 2022; MEWA, 2021).

The Wajid Aquifer System is situated within the Wajid Sandstone Formation, a component of the sedimentary rock layers across the Arabian Peninsula. This aquifer system is mainly composed of porous sandstone beds formed over millions of years. Typically deposited in old river channels, deltas, or coastal areas, these sandstone formations gradually solidify as sand grains bind together, forming a porous rock capable of storing and transmitting water. Meanwhile, the Umm Er Radhuma aquifer lies within the Umm Er Radhuma Formation, situated in the Arabian Peninsula. This aquifer system is primarily composed of carbonate rocks like limestone and dolomite, which have accumulated over extensive periods. These carbonate deposits typically stem from ancient marine settings, where sediments rich in calcium carbonate

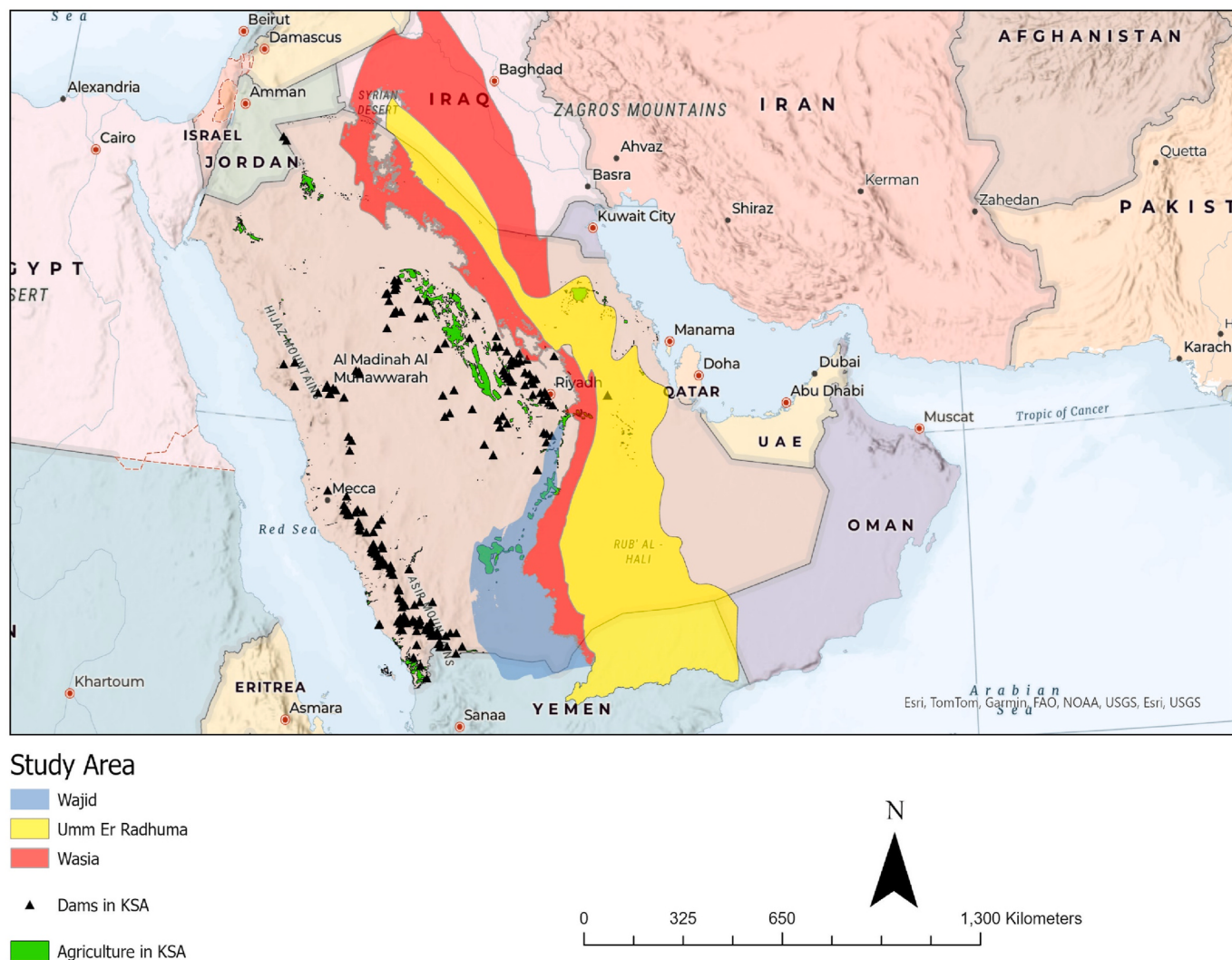


Fig. 1. Study Area: the locations of the three transboundary aquifer systems, Dams, and Agriculture in KSA.

Table 2

Aquifer Areas in each Arabian Peninsula country (MEWA, 2021).

Countries/Aquifer	Wajid (Area)	Umm Er Radhuma (Area)	Wasia (Area)
KSA	112038 km ² 90%	320480 km ² 69%	183010 km ² 52%
Yemen	12799 km ² 10%	106674 km ² 23%	2045 km ² 0.6%
Iraq	N/A	30805 km ² 7%	166269 km ² 47%
Oman	N/A	5457 km ² 1%	N/A
Syria	N/A	N/A	1298 km ² 0.4%
Total	124,837 km ²	463,416 km ²	352,622 km ²

settle and compress over time, forming porous and permeable layers of rock, renowned for its capacity to store and transmit groundwater. In addition, the Wasia Aquifer System is predominantly situated within the Wasia Formation, primarily composed of porous limestone and sandstone layers that have built up over millions of years. Originating from past marine settings, these sediments, such as sand and calcium carbonate, gather and compress over time, forming permeable rock layers. The porous quality of the limestone and sandstone enables the storage and movement of groundwater (GASTAT, 2022; MEWA, 2021).

2.2. Data and methods

2.2.1. GRACE & GRACE-FO derived Total Water Storage Anomalies data

GRACE detects spatiotemporal fluctuations in vertically integrated Total Water Storage (TWS). Variations in the GRACE-derived TWS indicate changes in one or more of the reservoirs listed below: snow/ice, surface water, soil moisture, groundwater, and wet biomass (Wahr et al., 1998). GRACE data have been widely utilized to calculate aquifer recharge and depletion rates (Ahmed et al., 2011, 2016; Al-Zyoud et al., 2015; Castellazzi et al., 2016; Chinnasamy and Agoramoorthy, 2015; Döll et al., 2014; Ellett et al., 2006; Fallatah et al., 2017; Feng et al., 2013; Huang et al., 2015; Jiang et al., 2016; Joodaki et al., 2014; Lezzaik and Milewski, 2018; Moghim, 2020; Saber et al., 2020). The monthly mass concentration GRACE and GRACE-FO derived Total Water Storage Anomaly (TWSA) datasets generated by the University of Texas, Center of Space Research (UT-CSR) with a spatial resolution of 0.25° x 0.25° has been utilized for this study (Table 3). A positive anomaly indicates water mass gain, and a negative value means mass loss. A simple seasonal decomposition method named STL (Seasonal and Trend decomposition using Loess) was used to fill out missing values and the gap between the GRACE and GRACE-FO mission observations.

2.2.2. GLDAS derived soil moisture storage anomaly (SMSA)

The Global Land Assimilation System (GLDAS) land surface model setup provides a worldwide dataset from 1948 that includes radiation, heat fluxes, hydrological components, and meteorological variables at 3-

hourly and monthly resolutions (Rodell et al., 2004; Rui and Beaudoin, 2020). This study utilizes monthly soil moisture anomalies from April 2002 to May 2021 (Table 3). To estimate soil moisture anomaly, a vital component of the TWS, we use the GLDAS-2.1 Noah land surface hydrology model at a monthly timestep. The Soil Moisture Storage (SMS) Anomaly can be estimated as the total summation of the outputs of soil moisture values of top four soil layers (0–10, 10–40, 40–100, and 100–200 cm). Groundwater Storage Anomaly is then computed based on the following equation:

$$\Delta GWSA = \Delta TWSA - \Delta SMSA \quad (1)$$

Where $\Delta GWSA$: is the change in groundwater storage anomalies, $\Delta TWSA$: is the change in terrestrial water storage anomalies, $\Delta SMSA$: is the change in soil moisture storage anomalies.

2.2.3. Field data

Agricultural data of 29 polygons (8665 Sq Km) distributed over the Wajid Aquifer system, 116 polygons (2161 Sq Km) distributed over the Umm er Radhuma Aquifer system, and 27 polygons (2870 Sq Km) distributed over the Wasia Aquifer system in Saudi Arabia were used to overlay agricultural water usage information over the groundwater source regions (Fig. 1). In addition, the locations of 213 dams over KSA were added to the geospatial analysis to overlay potential recharge inputs over the study area, as shown in Fig. 1. The data was maintained by the Ministry of Environment, Water, and Agriculture in the KSA, and collected and analyzed specifically for this study (Table 3).

2.2.4. Rainfall data

Rainfall data are used to explore the hydroclimatic controls on the temporal variations in the TWS observed over Wajid, Umm er Radhuma, and Wasia Aquifer systems. The monthly GLDAS Noah land surface model version 2.0 and version 2.1 were used in this study from Jan 1970 to May 2021 at a spatial resolution 0.25° x 0.25°. GLDAS Noah land surface model version 2.0 was used to provide data from Jan 1970 to Dec 2014 and GLDAS Noah version 2.1 was used to provide data from Jan 2000 to May 2021 (Table 3). After that, the average of overlapping data period was calculated over each aquifer.

3. Results

3.1. Terrestrial water storage anomalies by GRACE and GRACE-Follow on

The monthly regional mean of TWSA over the three transboundary aquifers was calculated from UT-CSR mascons for the study period April 2002 to May 2021 (Fig. 2). In the case of the Wajid Aquifer, the linear trend showed a decline rate of 2.14 cm/year, equivalent to about −0.87 km³/year. The trend at Umm Er Radhuma is estimated at a decline rate of 1.98 cm/year, which is about −2.79 km³/year, and the Wasia Aquifer is estimated at a decline rate of 3.11 cm/year, which is about −3.16 km³/year. Within the Wajid Aquifer, the northern part experienced maximal depletion, whereas the southern part shared with KSA and Yemen experienced minimal depletion. Wasia Aquifer results also indicate that the area of the southern part, which is shared with KSA and Yemen, experienced minimal depletion whereas the area center and northern part, which is shared with Iraq and a small part of Syria experienced maximal depletion. In the case of Wasia Aquifer, approximately 2870 Km² of irrigation is distributed over the entire aquifer in KSA, particularly in the central part of the aquifer. However, this area is also surrounded by large agricultural areas in the Riyadh, Alqassim, and Hail provinces. These agricultural zones, spanning an impressive 12,589 Km², are located approximately 40–50 km from the aquifer, relying on it for the essential pumping and transfer of water resources.

In addition, Umm Er Radhuma results indicate that the southern part of the aquifer area shared with Oman and Yemen experienced minimal

Table 3

The Datasets used in this study.

Variables	Sources and Processing	Units	Time
GRACE & GRACE-FO Terrestrial water storage (TWS)	Monthly average CSR (0.25° x 0.25°)	(cm)	April 2002 - May 2021
GLDAS Soil moisture storage (SMS)	NOAH model SMS for four layers (0–10, 10–40, 40–100, 100–200) Converted to anomaly (0.25° x 0.25°)	(cm)	April 2002 - May 2021
GLDAS-2.0 & GLDAS-2.1 Rainfall	NOAH model (0.25° x 0.25°)	(mm)	Jan 1970 - May 2021
Field Data	Dams and Agriculture by MEWA		2021

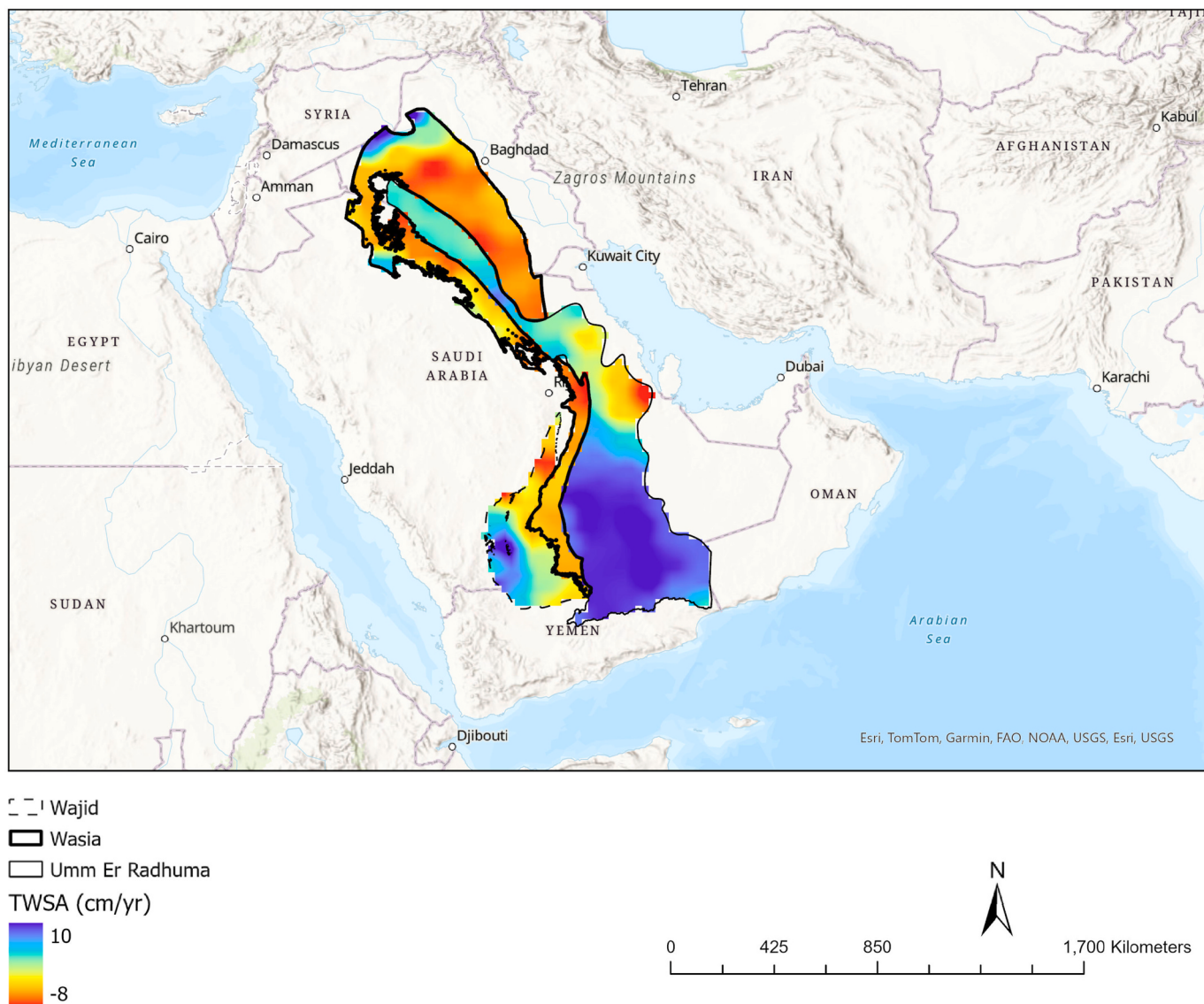


Fig. 2. Secular trend image of TWSA from GRACE and GRACE-FO generated from UT-CSR mascons dataset over the Arabian Peninsula from April 2002 to May 2022.

depletion and may have gained in total water storage. Furthermore, the area of the northern part, which is shared with Iraq, experienced minimal depletion. In contrast, most of the central parts of the aquifer near the capital city of Riyadh experienced high depletion rates. Overall, the southern part of our study region tends to have minimal depletion rates, around the border with Yemen and Oman, while the northern border regions shared between KSA, Iraq, and Syria and the central parts of the study region are experiencing maximum depletion (Fig. 2).

3.2. Gridded rainfall observations by GLDAS

Fig. 3(a and b and c) illustrates the temporal variations of rainfall over the study area during the time series. Our findings indicate that the total average of rainfall over Wasia received the highest quantity of average annual precipitation in the amount of 88.63 mm/year, Wajid received the amount of rainfall of 68.55 mm/year, while Umm Er Radhuma received the lowest annual average rainfall of 63.41 mm/year during the same time. Over the TBS under consideration, observations show that the wettest months are March and April, and the driest months are September and October; however, June to October are the driest months in the Wasia Aquifer region.

From temporal variations of total rainfall, there are three peaks

observed for Umm Er Radhuma, which were in 1976, 2018, and 2020; four peaks for Wasia, which were in 1972, 1982, 2018, and 2019; whereas six peaks for Wajid, which are in 1976, 1983, 1988, 1993, 2013, and 2016 (Fig. 3). The aquifers received the highest anomalous rainfall during these years compared to their low averages (Fig. 4). The annual average rainfall over Wasia shows two trends, until 1999, the rainfall decreased, but after 1999 the rainfall increased. In the case of Umm Er Radhuma, the rainfall dropped before 1990 and increased after 1990. Whereas for Umm Er Radhuma the rain had a long decrease until 2014, thereafter it has increased in recent years (Figs. 3 and 4).

3.3. Soil moisture storage anomaly (SMS) by GLDAS

The analysis of temporal variations in soil moisture anomaly for the top four layers over the study area illustrate the cyclic gain and loss moisture due to changes in rainfall (Fig. 5). The total average in the top layer of soil tends to decrease for the three aquifers, which reduces about -0.23 mm per year over Wajid, 0.20 mm per year over Umm Er Radhuma, and 0.04 mm per year over Wasia. The decline in the top layer shows the same driest and wettest seasons for every aquifer in terms of rainfall from April 2002 to May 2021, which corroborate our findings. Additionally, the results indicate an increase in soil moisture for

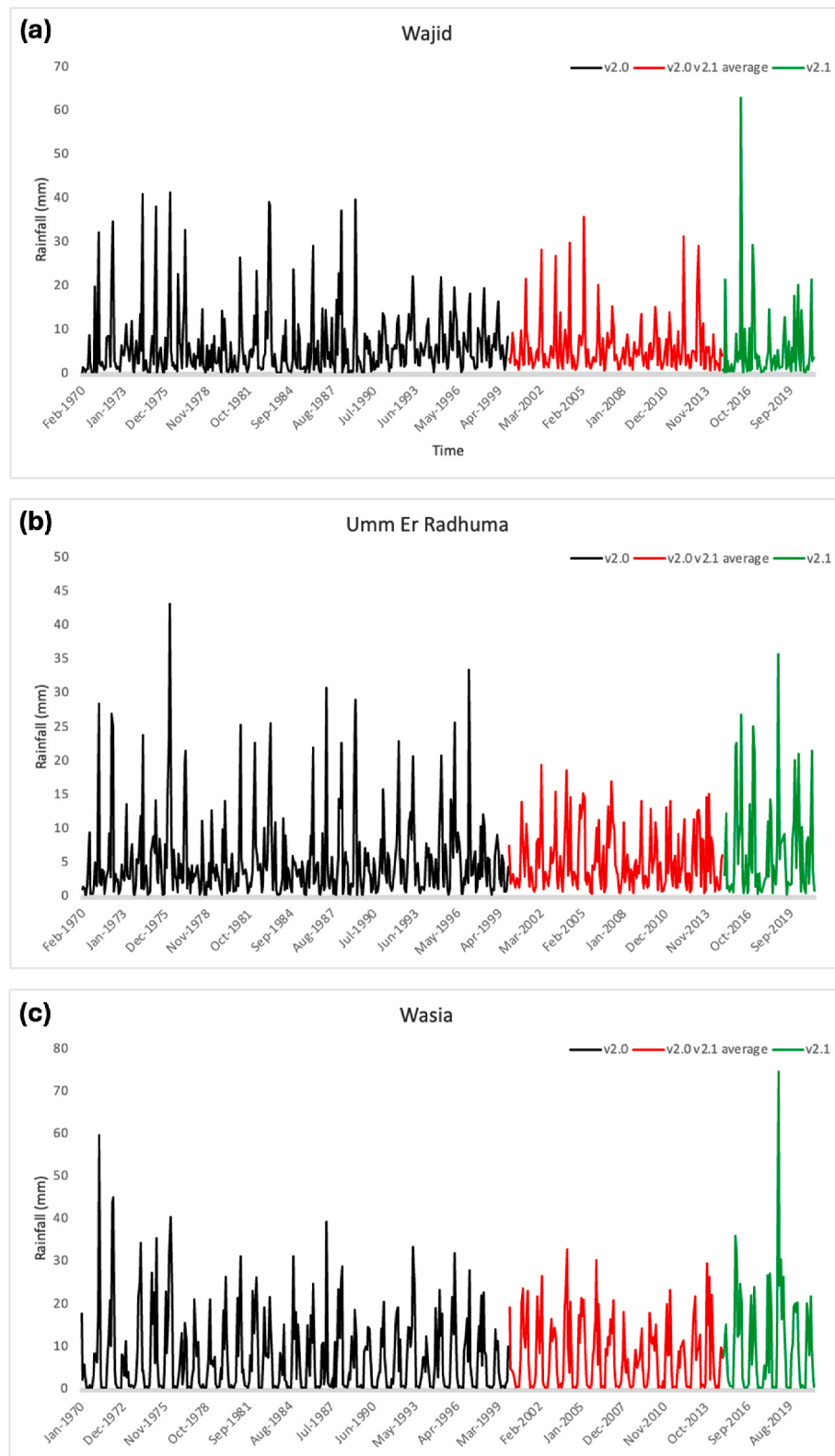


Fig. 3. Temporal variation in monthly rainfall extracted from GLDAS and averaged over (a) Wajid aquifer system (b) Umm Er Radhuma aquifer System, (c) Wasia aquifer system during Jan 1970–May 2021.

underneath layers for the whole aquifers during the time series (Table 4). The cumulative soil moisture volume in the top four layers were subtracted from the terrestrial water storage anomaly to obtain the groundwater storage anomaly (Equation (1)).

Moreover, our findings show a sharp decline in the annual soil

moisture amounts in the underneath layers from 2006 to 2012 over Wajid, and 2005 to 2012 over Umm Er Radhuma and Wasia. This trend can potentially be linked to past wheat production efforts in KSA during the study period (Ferragina and Canitano, 2014). Wheat is a water-intensive crop and necessitates massive quantities of groundwater

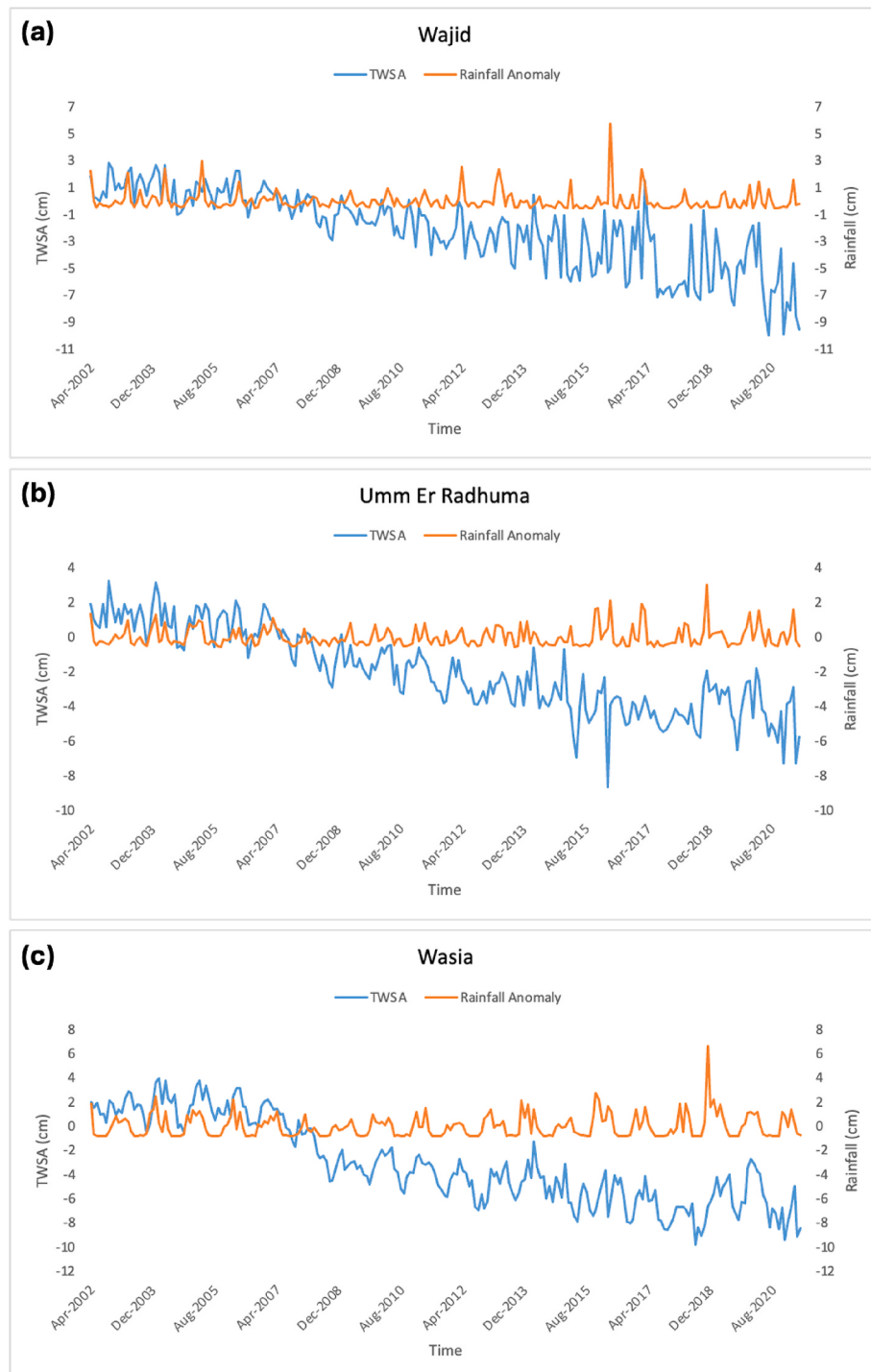


Fig. 4. Temporal variation anomalies in monthly TWS extracted from GRACE & GRACE-FO and Rainfall data averaged over the study area from April 2002–May 2021.

extraction ($\sim 1.0 \text{ km}^3/\text{year}$). Since 2000, the region has also seen significant growth of urbanization, construction of new transportation routes, agricultural expansion and accompanying irrigation projects (Fallatah et al., 2017). In 2008 however, KSA decided to abandon the project of becoming self-sufficient in wheat production in order to preserve groundwater sustainability. The country eventually ended its domestic wheat production programs in 2015 after more than thirty years (Miller magazine, 2016).

3.4. Groundwater storage anomalies (GWSA) by GRACE and GRACE-Follow on

Our study area is predominantly arid and semi-arid, with minimal surface water inputs. The observed TWS over Wajid, Umm Er Radhuma, and Wasia aquifers systems are connected to changes in soil moisture and groundwater storage. The GWS is quantified based on two parameters: the TWSA from GRACE and GRACE-FO observations, and the SMSA outputs from the GLDAS Noah model. The following equation represents groundwater storage:

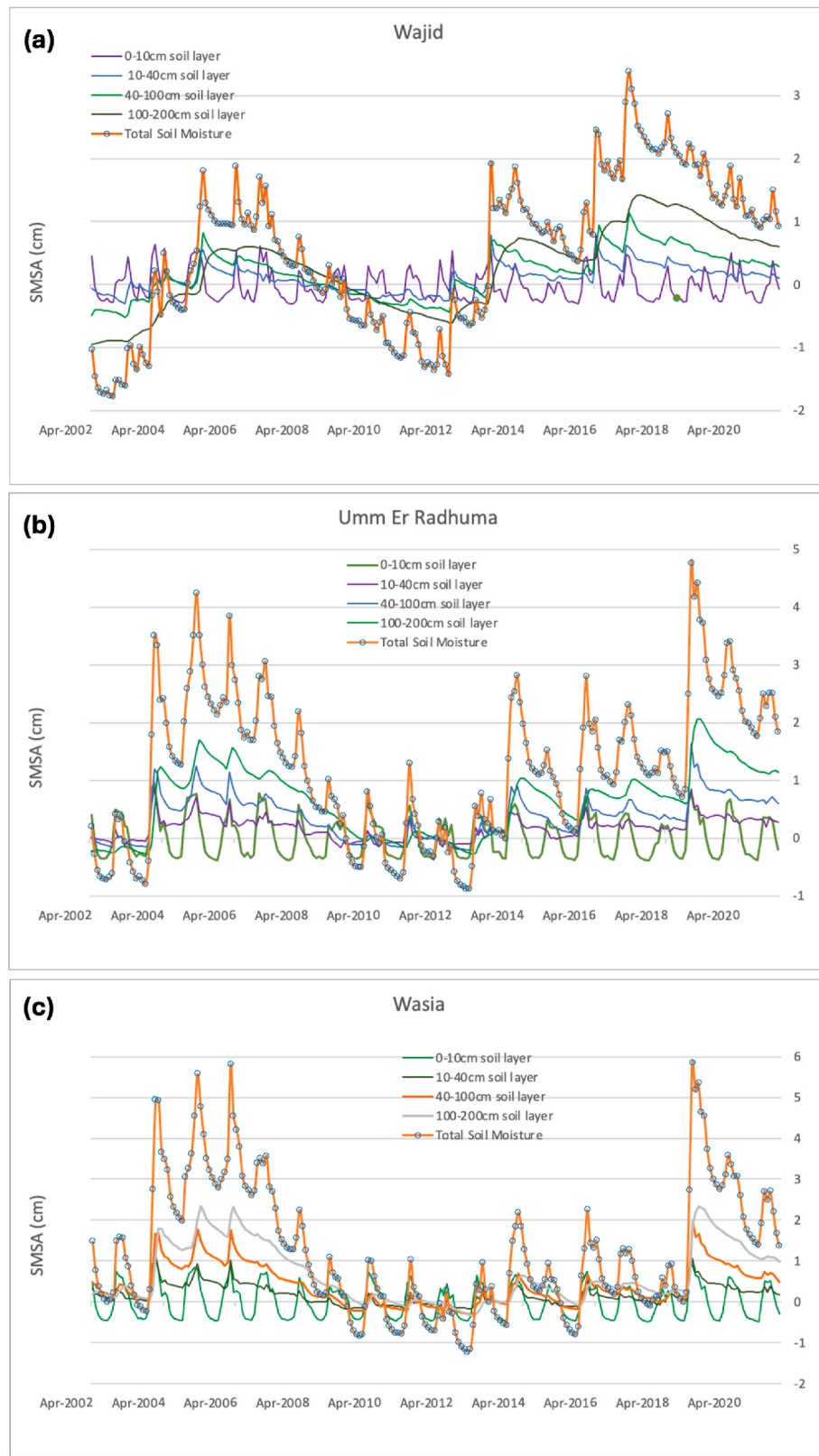


Fig. 5. Temporal variations in SMSA anomaly over the (a) Wajid, (b) Umm Er Radhuma, and (c) Wasia Aquifer systems, for four layers extracted from GLDAS during April 2002–May 2021.

$$\text{GWSA} = \text{TWSA} - \text{SMSA} \quad (2)$$

Where GWSA: is groundwater storage anomalies, TWSA: is terrestrial

water storage anomalies, SMSA: is soil moisture storage anomalies.

The results of the time series analysis revealed that groundwater storage declined in all aquifers from April 2002 to May 2021 is shown in Fig. 6. The Wasia shows greatest decline in groundwater storage at an

Table 4
SMSA of underneath layers over the study area.

SMSA Layer/Aquifer	Wajid (Unit)	Umm Er Radhuma (Unit)	Wasia (Unit)
10–40 cm	0.99 mm/yr	1.76 mm/yr	1.71 mm/yr
40–100 cm	1.82 mm/yr	3.68 mm/yr	3.95 mm/yr
100–200 cm	2.62 mm/yr	6.40 mm/yr	6.61 mm/yr
Total	5.43 mm/yr	11.84 mm/yr	12.27 mm/yr

average rate of -4.34 cm/year , which is equivalent to about $-2.92 \text{ km}^3/\text{year}$, while Umm Er Radhuma declined at the rate of approximately -3.18 cm/year ($-3.13 \text{ km}^3/\text{year}$), and Wajid at -2.65 cm/year ($-1.08 \text{ km}^3/\text{year}$) (Table 5). The spatial distribution of the GWSA results show minimal depletion in the southern border region of Saudi Arabia with Oman and Yemen, and the northwest border with Jordan and Syria (Fig. 7). However, rapid groundwater storage depletion can be seen in central Saudi Arabia (near the capital region of Riyadh) and in the northern border areas with Iraq and Kuwait. Our results thus show strong spatiotemporal variations in all three transboundary aquifer systems across Saudi Arabia and in regions shared with most of its neighboring countries in the Arabian Peninsula.

4. Discussion and conclusions

Groundwater is a critical freshwater source in the arid and semi-arid regions of the Arabian Peninsula countries. Most groundwater sources in this region are transboundary aquifers, which have no groundwater sharing or management treaty governing them. As the region is undergoing rapid population growth, unilateral agricultural and urban development projects have drastically increased the demand and usage for groundwater in recent decades. Sustainable management of this critical resource and efficient usage of major aquifer systems are thus key concerns for the region.

In this study, we develop and apply an integrated approach using remote sensing and geophysical observations to quantify the groundwater depletion rates of major transboundary aquifers and examine the natural and anthropogenic drivers of water storage variations over a two-decade period – April 2002 to May 2021 – in the Arabian Peninsula region. We combine earth observations such as Gravity Recovery and Climate Experiment (GRACE) and GRACE-FO (Follow-On), land surface hydrological modeling using the Global Land Data Assimilation Systems (GLDAS), and local water resources infrastructure and usage information to investigate the spatiotemporal variations in the groundwater

resources over the Wajid, Umm Er Radhuma, and Wasia transboundary aquifer systems shared between Saudi Arabia, Iraq, Yemen, Oman, and Syria.

Our results show extensive and consistent groundwater depletion in central and northern Saudi Arabia bordering Iraq, while improvements in groundwater storage in the south near the borders with Yemen and Oman. All three aquifers are witnessing significant Total Water Storage (TWS) and Ground Water Storage (GWS) depletion. The largest declines of TWS and GWS were in Wasia aquifer at $-3.11 \text{ cm per year}$ and $-4.34 \text{ cm per year}$, respectively. Umm Er Radhuma is witnessing significant negative variations of $-1.98 \text{ cm per year}$ and $-3.18 \text{ cm per year}$. In contrast, Wajid is experiencing the least negative variations of TWS and GWS at $-2.14 \text{ cm per year}$ and $-2.65 \text{ cm per year}$, respectively. During the same time period of time, the total average rainfall over Wasia received the highest quantity of rainfall of 7.47 mm/month , Wajid received an amount of rainfall of 5.78 mm/month , while Umm Er Radhuma received the lowest annual average rainfall of 5.34 mm/month .

The observed negative trend anomalies over the study area are being influenced by natural factors, such as overall climate change and associated changes in precipitation rate, and anthropogenic factors, such as increased groundwater extraction for urbanization and irrigation activities. In this study, the field data on agricultural and water resources infrastructure collected from KSA (Fig. 1) are used to validate the earth observations since most of the study area is located inside KSA (Fig. 3). Based on our estimation, approximately 8665 Km^2 of irrigation is distributed over the three focus aquifers, primarily located in the northern parts of the KSA. As GRACE data indicates, there is intensive use of TWS in the northern part of the Wajid aquifer, presumably due to large scale agriculture. Within the Umm Er Radhuma Aquifer, approximately 2162 Km^2 of irrigation is located, where groundwater is withdrawn, mostly from the center part of the aquifer. Analysis of satellite

Table 5
GWSA over the study area.

Aquifer/GWSA	Average	1st sharp decline	2nd sharp decline
Wajid	$-2.65 \text{ cm/yr} (-1.08 \text{ km}^3/\text{year})$	2003–2008 0.12 cm/yr	2010–2021 -4.63 cm/yr
Umm Er Radhuma	$-3.18 \text{ cm/yr} (-3.13 \text{ km}^3/\text{year})$	2002–2012 -1.28 cm/yr	2013–2019 -6.83 cm/yr
Wasia	$-4.34 \text{ cm/yr} (-2.92 \text{ km}^3/\text{year})$	2003–2009 -1.51 cm/yr	2010–2020 -6.14 cm/yr

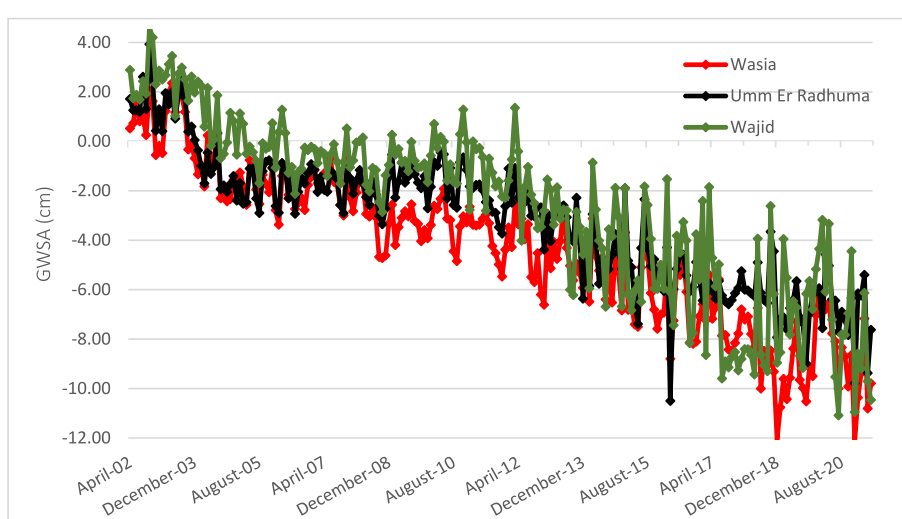


Fig. 6. Groundwater storage anomalies for the study area, showing the variability from April 2002–May 2021.

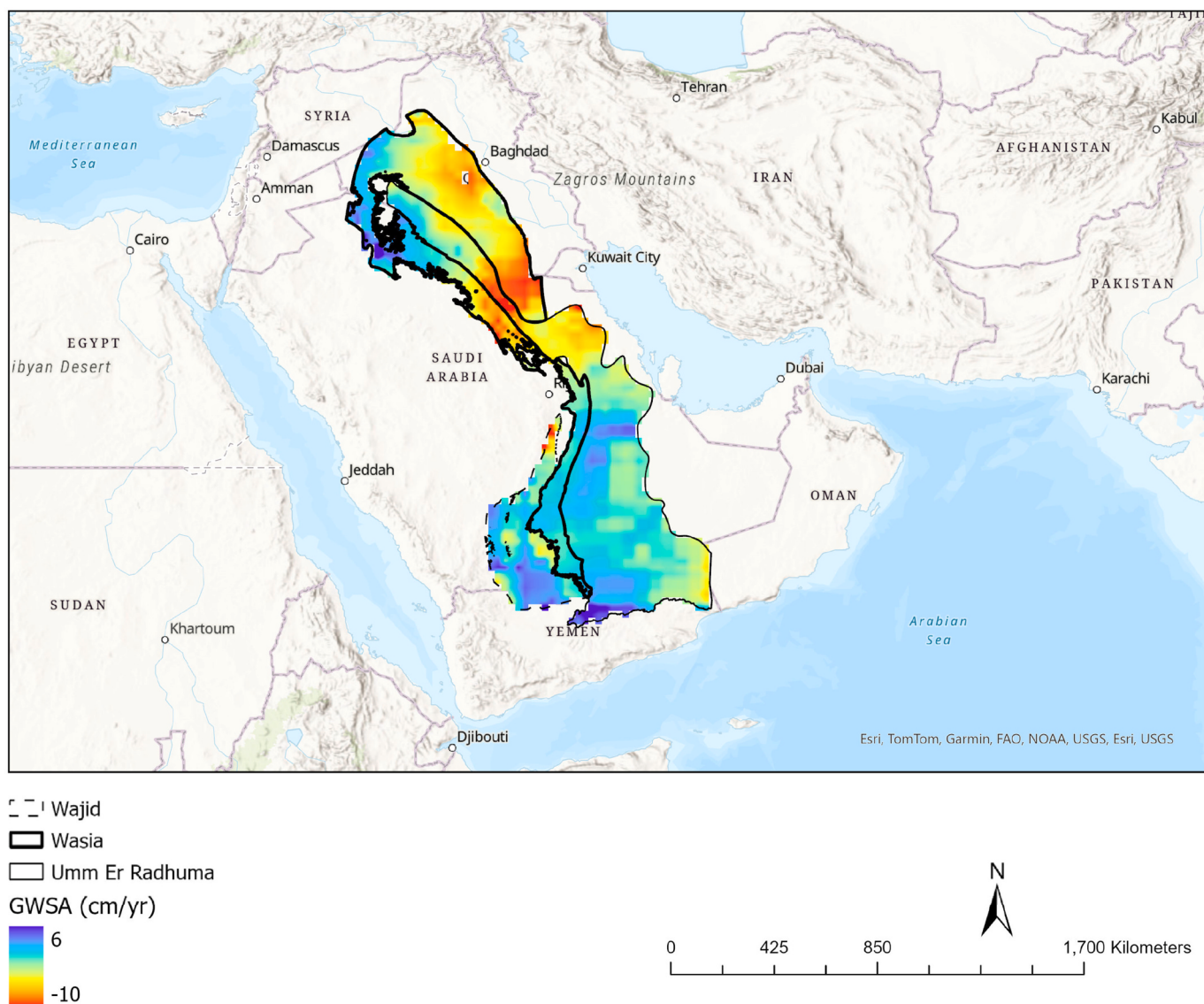


Fig. 7. Calculated Groundwater storage anomaly trends from GRACE and GRACE-FO and GLDAS variables.

data confirms that the central parts of this aquifer are experiencing the highest depletion during the study period (Fig. 7). The figure also shows a significant amount of depletion around Baghdad, the capital city of Iraq – confirming the robustness of this approach for monitoring groundwater storage over large areas as the importance of information exchange and cooperation over these transboundary aquifers.

The findings of this study illustrated the potential of using remote sensing earth observations in conjunction with ground-based datasets and modeling outputs to monitor past and present changes in water storage depletion, time-series patterns, and long-term trends in the vital groundwater resources of this region. However, there are two limitations that should be understood along with the merits of this approach. One, the spatial resolution of the GRACE and GRACE-FO data sources are of coarse nature by design and provide a large-scale picture of total water storage of an area. Thus, it should be interpreted and understood along with more detailed information on local scale variations, demands, and withdrawals of water resources. Two, the downscaling processes employed by research institutions to use the GRACE and GRACE-FO gravity datasets add uncertainty to the mass concentration solutions and increase the room for error. However, the $0.25^\circ \times 0.25^\circ$ solution prepared by CSR are known to be the most accurate and highest resolution dataset appropriate for this study.

Saudi Arabia has launched a 2030 vision and roadmap for economic, social, and institutional reforms to alter the country into a lively and sustainable society. The vision seeks to enhance the quality of life for Saudi citizens and residents, attract investments, and assemble new job opportunities (CEDA, 2016). This huge project is expected to significantly increase water demand and might cause extreme groundwater depletion unless Saudi Arabia and the neighboring countries sharing these transboundary aquifers make collaborative policies to preserve the groundwater resources. This study will help ensure that the Wajid, Umm Er Radhuma, and Wasia aquifers' water resources are monitored and utilized effectively and efficiently, and to support the sustainable development and management of the Arabian Peninsula's natural resources.

CRediT authorship contribution statement

Mohammed O. Altayyar: Writing – review & editing, Writing – original draft, Validation, Supervision, Software, Resources, Project administration, Methodology, Data curation, Conceptualization. **Shoaib Ali:** Writing – review & editing, Validation, Software, Methodology, Investigation. **Albert E. Larson:** Software, Methodology, Data curation. **Thomas Boving:** Writing – review & editing. **Leon Thiem:** Writing –

review & editing. **Ali S. Akanda:** Writing – review & editing, Investigation, Funding acquisition.

Declaration of competing interest

The authors declare no competing interests.

Data availability

Data will be made available on request.

Acknowledgements

The authors greatly acknowledge the Saudi Arabian Cultural Mission (SACM) and the National Center for Environmental Compliance (NCEC) of Saudi Arabia for supporting the doctoral work of Mohammed Altayyar through a governmental scholarship program and data access facilities, respectively. This study was also supported, in part, by a grant from NASA Earth Action: Health and Air Quality (Ali S Akanda; Grant: 80NSSC22K1044).

References

- Abdulrazzak, M.J., Oikonomou, P.D., Grigg, N.S., 2020. Transboundary groundwater cooperation among countries of the Arabian Peninsula. *J. Water Resour. Plann. Manag.* 146 (1) [https://doi.org/10.1061/\(asce\)wr.1943-5452.0001140](https://doi.org/10.1061/(asce)wr.1943-5452.0001140).
- Ahmed, M., Sultan, M., Wahr, J., Yan, E., Milewski, A., Sauck, W., Becker, R., Welton, B., 2011. Integration of GRACE (Gravity Recovery and Climate Experiment) data with traditional data sets for a better understanding of the time-dependent water partitioning in African watersheds. *Geology* 39 (5). <https://doi.org/10.1130/G31812.1>.
- Ahmed, M., Sultan, M., Yan, E., Wahr, J., 2016. Assessing and improving land surface model outputs over Africa using GRACE, field, and remote sensing data. *Surv. Geophys.* 37 (Issue 3) <https://doi.org/10.1007/s10712-016-9360-8>.
- Al-Zyoud, S., Rühaak, W., Forootan, E., Sass, I., 2015. Over exploitation of groundwater in the centre of amman zarqa basin-Jordan: evaluation of well data and GRACE satellite observations. *Resources* 4 (4). <https://doi.org/10.3390/resources4040819>.
- Alfaifi, H.J., Abdelfatah, M.S., Abdelrahman, K., Zaidi, F.K., Ibrahim, E., Alarifi, N.S., 2017. Groundwater management scenarios for the Biyadh-Wasia aquifer systems in the eastern part of Riyadh region, Saudi Arabia. *J. Geol. Soc. India* 89 (6). <https://doi.org/10.1007/s12594-017-0676-x>.
- Almazroui, M., Islam, M.N., Saeed, S., Saeed, F., Ismail, M., 2020. Future changes in climate over the Arabian Peninsula based on CMIP6 multimodel simulations. *Earth Systems and Environment* 4 (4). <https://doi.org/10.1007/s41748-020-00183-5>.
- Brown, G.F., Schmidt, D.L., Huffman, A.C., 1989. Geology of the Arabian Peninsula: Shield Area of Western Saudi Arabia, vol. 560 A. US Geological Survey Professional Paper. <https://doi.org/10.3133/pp560A>.
- Castellazzi, P., Martel, R., Galloway, D.L., Longuevergne, L., Rivera, A., 2016. Assessing groundwater depletion and dynamics using GRACE and InSAR: potential and limitations. *Groundwater* 54 (Issue 6). <https://doi.org/10.1111/gwat.12453>.
- CEDA (2016). Council of Economic and Development Affairs, Kingdom of Saudi Arabia. Vision 2030. Available at: <https://vision2030.gov.sa/en> [Accessed June 06, 2023].
- Chinnasamy, P., Agoramoorthy, G., 2015. Groundwater storage and depletion trends in Tamil Nadu state, India. *Water Resour. Manag.* 29 (7) <https://doi.org/10.1007/s11269-015-0932-z>.
- Döll, P., Müller Schmied, H., Schuh, C., Portmann, F.T., Eicker, A., 2014. Global-scale assessment of groundwater depletion and related groundwater abstractions: combining hydrological modeling with information from well observations and GRACE satellites. *Water Resour. Res.* 50 (7) <https://doi.org/10.1002/2014WR015595>.
- Edgell, H.S., 2006. Arabian deserts: nature, origin, and evolution. <https://doi.org/10.1071/4020-3970-0>.
- Ellett, K.M., Walker, J.P., Western, A.W., Rodell, M., 2006. A framework for assessing the potential of remote-sensed gravity to provide new insight on the hydrology of the Murray-Darling Basin. *Aust. J. Water Resour.* 10 (2) <https://doi.org/10.1080/13241583.2006.11465286>.
- Fallatah, O.A., Ahmed, M., Save, H., Akanda, A.S., 2017. Quantifying temporal variations in water resources of a vulnerable middle eastern transboundary aquifer system. *Hydrol. Process.* 31 (23) <https://doi.org/10.1002/hyp.11285>.
- Fallatah, O.A., Ahmed, M., Cardace, D., Boving, T., Akanda, A.S., 2019. Assessment of modern recharge to arid region aquifers using an integrated geophysical, geochemical, and remote sensing approach. *J. of Hydrology* 569. <https://doi.org/10.1016/j.jhydrol.2018.09.061>.
- Famiglietti, J.S., 2014. The global groundwater crisis. *Nat. Clim. Change* 4 (1). <https://doi.org/10.1038/nclimate2425>.
- Famiglietti, J.S., Rodell, M., Durack, P.J., Trenberth, K.E., Held, I.M., Soden, B.J., Tiwari, V.M., Wahr, J., Swenson, S., Scanlon, B.R., Voss, K.A., Tapley, B.D., Reager, J.T., Famiglietti, J.S., Houborg, R., Blunden, J., Arndt, D.S., Zaitchik, B.F., Swenson, S.C., et al., 2013. Environmental science. Water in the balance. *Science* (New York, N.Y.) 340 (6138). <https://doi.org/10.1126/science.1236460>.
- Feng, W., Zhong, M., Lemoin, J.M., Biancale, R., Hsu, H.T., Xia, J., 2013. Evaluation of groundwater depletion in North China using the Gravity Recovery and Climate Experiment (GRACE) data and ground-based measurements. *Water Resour. Res.* 49 (4) <https://doi.org/10.1002/wrcr.20192>.
- Ferragina, E., Canitano, G., 2014. Water and food security in the arab countries: national and regional implications. *Global Environment* 7 (2). <https://doi.org/10.3197/ge.2014.070204>.
- GASTAT (2022). General Authority for Statistics, Kingdom of Saudi Arabia. Available at: <https://www.stats.gov.sa/en> [Accessed 15 December 2022].
- Huang, Z., Pan, Y., Gong, H., Yeh, P.J.F., Li, X., Zhou, D., Zhao, W., 2015. Subregional-scale groundwater depletion detected by GRACE for both shallow and deep aquifers in North China Plain. *Geophys. Res. Lett.* 42 (6) <https://doi.org/10.1002/2014GL062498>.
- Jasechko, S., Seybold, H., Perrone, D., et al., 2024. Rapid groundwater decline and some cases of recovery in aquifers globally. *Nature* 625, 715–721. <https://doi.org/10.1038/s41586-023-06879-8>.
- Jiang, Q., Ferreira, V.G., Chen, J., 2016. Monitoring groundwater changes in the Yangtze River basin using satellite and model data. *Arabian J. Geosci.* 9 (7) <https://doi.org/10.1007/s12517-016-2522-7>.
- Joodaki, G., Wahr, J., Swenson, S., 2014. Estimating the human contribution to groundwater depletion in the Middle East, from GRACE data, land surface models, and well observations. *Water Resour. Res.* 50 (3) <https://doi.org/10.1002/2013WR014633>.
- Khogali, A., Birkle, P., Al-Shaibani, A., Keller, M., Tawabini, B., Makkawi, M., 2020. Geochemical assessment of potential sources for nitrate in the wasia aquifer, Al Kharj Area, central Saudi Arabia. *Water* 12 (5). <https://doi.org/10.3390/w12051479>.
- Kinzelbach, W., Aeschbach, W., Alberich, C., Goni, I.B., Beyerle, U., Brunner, P., Chiang, W.-H., Rueedi, J., Zoellmann, K., 2002. A survey of methods for analysing groundwater recharge in arid and semi-arid regions. In: Early Warning and Assessment Report Series (Issue UNEP/DEWA/RS.02-2). <https://climate-adapt.eea.europa.eu/en/metadata/organisations/division-of-early-warning-and-assessment-de-wa-unep>.
- Lezzaik, K., Milewski, A., 2018. A quantitative assessment of groundwater resources in the Middle East and North Africa region. *Hydrogeol. J.* 26 (1) <https://doi.org/10.1007/s10040-017-1646-5>.
- Liuzzo, L., Noto, L.V., Arnone, E., Caracciolo, D., La Loggia, G., 2015. Modifications in water resources availability under climate changes: a case study in a Sicilian basin. *Water Resour. Manag.* 29 (4) <https://doi.org/10.1007/s11269-014-0864-z>.
- Mechlem, K., 2011. Past, present and future of the international law of transboundary Aquifers. *Int. Community Law Rev.* 13 (Issue 3) <https://doi.org/10.1163/18719731X582278>.
- MEWA (2021). Ministry of Environment, Water and Agriculture, Kingdom of Saudi Arabia. Available at: <https://mewa.gov.sa/en/Ministry/Pages/default.aspx> [Accessed 4 October 2021].
- Moghim, S., 2020. Assessment of water storage changes using GRACE and GLDAS. *Water Resour. Manag.* 34 (2) <https://doi.org/10.1007/s11269-019-02468-5>.
- Mohammadmazdeh-Habili, J., Khalil, D., 2020. Assessment of artificial recharge dams and improvement of their groundwater-recharge capacity. *J. Hydrol. Eng.* 25 (5) [https://doi.org/10.1061/\(asce\)he.1943-5584.0001909](https://doi.org/10.1061/(asce)he.1943-5584.0001909).
- Othman, A., Sultan, M., Becker, R., Alsefry, S., Alharbi, T., Gebremichael, E., Alharbi, H., Abdellah, K., 2018. Use of geophysical and remote sensing data for assessment of aquifer depletion and related land deformation. *Surv. Geophys.* 39 (Issue 3) <https://doi.org/10.1007/s10712-017-9458-7>.
- Rodell, M., Houser, P.R., Jambor, U., Gottschalck, J., Mitchell, K., Meng, C.J., Arseneault, K., Cosgrove, B., Radakovich, J., Bosilovich, M., Entin, J.K., Walker, J.P., Lohmann, D., Toll, D., 2004. The global land data assimilation system. *Bull. Am. Meteorol. Soc.* 85 (3) <https://doi.org/10.1175/BAMS-85-3-381>.
- Rui, H.L., Beaudoin, H., 2020. README document for NASA GLDAS version 2 data products. Goddard Earth Sciences Data and Information Services Center (GES DISC) 16 (1). https://hydro1.gesdisc.eosdis.nasa.gov/data/GLDAS/README_GLDAS2.pdf.
- Saber, M., Kantoush, S.A., Sumi, T., 2020. Assessment of spatiotemporal variability of water storage in Arabian countries using global datasets: implications for water resources management. *Urban Water J.* 17 (5) <https://doi.org/10.1080/1573062X.2020.1713174>.
- Scanlon, B.R., Healy, R.W., Cook, P.G., 2002. Choosing appropriate techniques for quantifying groundwater recharge. *Hydrogeol. J.* 10 (1) <https://doi.org/10.1007/s10040-001-0176-2>.
- Sultan, M., Sturchio, N., Al Seify, S., Milewski, A., Becker, R., Nasr, I., Sagintayev, Z., 2008. Geochemical, isotopic, and remote sensing constraints on the origin and evolution of the Rub Al Khali aquifer system, Arabian Peninsula. *J. Hydrol.* 356 (1–2) <https://doi.org/10.1016/j.jhydrol.2008.04.001>.
- Vegetation of the Arabian Peninsula, 1998. In: Vegetation of the Arabian Peninsula <https://doi.org/10.1007/978-94-017-3637-4>.
- Wahr, J., Molenaar, M., Bryan, F., 1998. Time variability of the Earth's gravity field: hydrological and oceanic effects and their possible detection using GRACE. *J. Geophys. Res. Solid Earth* 103 (B12). <https://doi.org/10.1029/98jb02844>.